UNIVERSITA' DEGLI STUDI DI PARMA
DOTTORATO DI RICERCA IN NEUROSCIENZE
XXVIII CICLO

Proactive and reactive inhibition during overt and covert actions. An electrical neuroimaging study

Coordinatore:

Chiar.mo Prof. Vittorio Gallese

Tutor:

Chiar.mo Prof. Vittorio Gallese

Dottoranda: *Dott.ssa Monica Angelini*

INDEX

Chapter 1

Introduction

1.1 Proactive and reactive response inhibition and related neural networks

Response inhibition is the ability to suppress inadequate but automatically activated, prepotent or ongoing response tendencies [for review, see 1]. In the framework of cognitive control in general [2] and of motor inhibition in particular [3], two distinct operating strategies have been described: “proactive” and “reactive” control modes. In the proactive modality, inhibition or, more generally speaking, planned action strategies, are recruited in advance by predictive external cues or by endogenous signals, and actively maintained before their enactment, in order to optimize performance in a goal-driven manner. Hence, proactive inhibition is a top-down form of control that is used when actions have to be restrained in anticipation of inhibition and that results in slowing down or temporarily holding response tendencies. Conversely, in the reactive control mode, cognitive resources in general and inhibition in particular, are phasically enacted after the detection of the cognitive demanding or inhibitory signals. Hence, reactive inhibition is a bottom-up form of control, triggered after a salient external event occurred and used when actions need to be inhibited outright.

Regarding the cerebral mechanisms underpinning motor inhibition, ample evidence points to a core circuit for reactive control requiring functional integration of frontal cortex regions, basal ganglia (BG) and the thalamus, to modulate subcortical input to cortical motor areas, with the primary motor cortex (M1) as a final target. Within this fronto-BG network, the right inferior frontal gyrus (rIFG), the presupplementary motor area (pre-SMA), the striatum and

the subthalamic nucleus (STN) would play a pivotal role [for review, see 3]. Among different anatomical pathways connecting these cerebral regions [4, 5], while response execution is enabled by the direct corticostriatal pathway, successful inhibition might be mediated by either the hyperdirect or the indirect pathways [3]. In particular, it has been proposed that the hyperdirect pathway mediates a rapid "global stopping", clearing all motor responses, through the subthalamic nucleus (STN) which receives direct input by the IFG and pre-SMA and sends massive output to the globus pallidus pars interna (GPi). The STN sends diffuse excitatory projections to the output nuclei of the BG, which in turn have inhibitory connections with motor thalamic nuclei. During reactive inhibition, STN activity could broadly reduce thalamic drive to the motor system and quickly inhibit ongoing responses. As a counterpart, the hyperdirect pathway lacks specificity on the inhibited responses, due to the wide distribution of its outputs on the GPi.

Conversely, the indirect pathway through the striatum would mediate a "selective" stopping, i.e., a mechanism with specific inhibitory effects, suppressing thalamocortical projections directed at definite M1 motor representations [3]. Along the indirect pathway, the striatum and then the globus pallidus pars externa (GPe) and STN are involved before the output nuclei of the BG. Due to the high degree of specificity of the STN projections to GPi along this pathway, the indirect cortico-BG circuit could exert a focused inhibitory effect on specific responses, without globally interrupting other ongoing movements.

Notwithstanding the amount of evidence supporting this hypothesized inhibitory network, several questions remain open. First, the exact role and hierarchical interactions between principal cerebral nodes of the network during reactive inhibition are still highly debated. Indeed, it has been proposed that the rIFG could be more involved in stimulus-driven attention and in the detection of the inhibitory signal, or in updating and shifting between response plans [e.g., 6] rather than in directly implementing inhibition. Regarding the pre-

SMA, the multiplicity of its proposed roles in motor control (ranging from action selection, switching between action plans or task sets, to motor inhibition) [7, 8], has been summarized in one fundamental function: the resolution of conflict between competitive response plans such as responding and inhibiting the response [7, 9]. Interestingly, it has been suggested that motor inhibition and response selection could in fact represent merely different descriptions of the same processes, emerging from a single neural mechanism and involving the same cortical areas that would mediate both processes [8]. In this framework, the pre-SMA would coordinate both the response inhibition and the preparatory selection of actions by means of the same looped interconnections with the BG. The pre-SMA is thought to act principally through the BG circuits, engaged via direct pre-SMA-BG connections, or alternatively by the recruitment of other prefrontal areas, such as the rIFG. In this regard, the functional hierarchy between the pre-SMA and the rIFG remains an open issue. On the one hand, some lines of evidence point to the fact that the rIFG could influences M1 indirectly, via the pre-SMA [e.g., 10]; on the other hand, the opposite pattern of functional interaction, with a leading inhibitory role of the rIFG, has been proposed [e.g., 11]. In addition, the necessary involvement of the BG in reactive inhibition has been questioned, given that several studies showed that the rIFG and the pre-SMA can exert direct influence on M1, bypassing the BG [12, 13].

In the context of response inhibition, both the proposed global and the selective inhibitory mechanisms and related underlying cerebral networks not only can be reactively triggered at the presentation of the inhibitory signals, but also can be preactivated when inhibitory signals can be anticipated (proactive inhibition) [3]. Of note, functional magnetic resonance imaging (fMRI) studies have shown that cerebral activations during proactive and reactive inhibition largely overlaps [14-18], with a shared engagement of frontoparietal circuits and BG, mainly in the right hemisphere. These findings suggest that at least part of the neural network for reactive inhibition could be recruited in advance [3], priming cortical regions in preparation

for the upcoming inhibition and influencing the efficiency of inhibitory control. Nevertheless, the overlapping of proactively and reactively engaged inhibitory areas is only partial, with some brain regions selectively associated with each of these mechanisms [14, 16-18]. In this regard, the exact role of the rIFG, pre-SMA and different BG in proactive inhibition is still unclear. Some of the pivotal nodes of the reactive inhibitory circuit (namely, the pre-SMA and the striatum) seems to play similar functions of selection between conflicting response plans also during proactive inhibition. Conversely, since the main role of the rIFG in reactive inhibition has been related to the detection of the inhibitory signal and with the triggering of the inhibition process during the updating of response plans [19], its engagement in proactive inhibition remains debated. Indeed, while some studies showed the activation of the rIFG in preparation to stop a response [e.g., 15, 20], others did not find its involvement in proactive inhibition [e.g., 14, 16-18]. Furthermore, the relative contribution of different cortical-BG circuits to reactive or proactive inhibitory mechanisms remains unclear. It has been proposed that reactive inhibition would principally rely on rIFG, STN and the hyperdirect BG circuit, and that the striatum is not involved in reactive inhibition [21]. Nevertheless, both these frontal-BG circuits could take part in proactive as well as reactive control. Computational theories of the speed-accuracy trade-off propose that increased accuracy can be achieved by preactivating the global inhibitory network via modulating cortical input to the STN [22]. Conversely, proactive selective inhibition would be implemented in the presence of information in working memory about particular response tendencies needed to be controlled in the future, when the inhibitory goal is known in advance. The dorsolateral prefrontal cortex (DLPFC), in particular the middle frontal gyrus, would build-up a “top-down inhibitory set” on the striatum and on the indirect BG loop: this mechanism could apply advance control onto a specific motor representation, possibly by modulating the response threshold in M1. Later

on, this prepared control would be actually implemented (i.e., applied on motor output), at the onset of the inhibitory signal [3].

Recent evidence showed that although proactive and reactive forms of inhibition seem to activate the same core networks, further additional areas are selectively engaged and uniquely associated with each of these mechanisms [18]. In particular, it has been shown that the superior parietal lobule (SPL), dorsal premotor cortex (dPMC) and putamen form a functionally coherent network specifically associated with proactive inhibition, likely exerting top-down influence over motor preparation. Conversely, two right lateralized networks were associated with reactive inhibition (intended as stimulus-driven action cancelation). In particular, a right-lateralized network including the DLPFC and the inferior parietal lobule (IPL) would be involved in stimulus-driven attentional control, responding to the inhibitory signal requiring task-goal updating (e.g., stopping a prepared response). Successively, a right-lateralized circuit including the ventrolateral prefrontal cortex (VLPFC) and the pre-SMA would implement the switching from an intended action to an inhibitory response [18].

Another cortical area that plays a pivotal role in motor control is the dPMC. This area would be relevant not only for conditional motor behaviour, in which actions are selected on the basis of arbitrary sensory stimuli [23], but also for motor inhibition. The inhibitory role of the dPMC has been put forward by neuronal recordings in monkeys during a countermanding/Stop reaching task [24]. This study identified a population of reaching-related neurons, showing a pattern of activity that correlated with the suppression of programmed arm movements.

Furthermore, in humans the dPMC is one of the so-called “negative motor areas” (NMAs), i.e., cortical regions whose electrical stimulation induces the inability to perform voluntary movements or sustained muscle contraction, without concomitant disturbance of consciousness [25]. Of note, the dPMC would play a relevant role also in proactive inhibition.

Indeed, single-unit recordings in monkeys showed that during the foreperiod of a cued Go/NoGo task, dPMC neurons signalled more NoGo than Go responses [26].

1.2 Electrophysiological indexes of response inhibition

One of the most used paradigm to study motor inhibition is the Go/NoGo task, based on a choice-reaction time task requiring a response-selection process between either executing or withholding a motor response, as respectively instructed by a "Go" or a "NoGo" stimulus. Since during this task, there is a bias towards responding, NoGo trials are associated with the activation of inhibitory process to withhold the prepared prepotent Go response. However, such task requests not only response inhibition, but taps into different cognitive functions, including stimulus-driven reorienting of attention, working memory, decision making and response selection. Indeed, motor inhibition should not be considered as arising only from neural inhibitory mechanisms, but rather as resulting from a balance between activation and inhibition processes: accordingly, inhibitory processes are difficult to disentangle from response selection, motor planning and programming and error monitoring. This could justify the large number of structures that has been identified in fMRI studies using Go/NoGo task, including bilateral DLPFC and VLPFC, the pre-SMA, the dorsal anterior cingulate cortex (dACC), bilateral SPL and IPL, and the BG [for review, see 27]. Of note, the lack of specificity of paradigms such as the Go/NoGo task, that do not measure pure forms of inhibition but also other related cognitive processes, does not necessarily decrease the usefulness of these behavioural tasks. Indeed, both motor inhibition and interrelated cognitive processes could altogether substantially contribute to successful behavioural control.

In order to evaluate proactive and reactive inhibition, cued variants of the Go/NoGo task, such as the Continuous Performance Task (CPT)-OX paradigm, are used [28]. Basic CPTs [29]

consist of rapid presentation of constantly changing stimuli with a specific low frequency "target" stimulus. Requesting the detection and the response to the infrequent target, CPTs evaluate selective and sustained attention, working memory, and reactive response inhibition [28]. Cued versions of CPT introduce a warning stimulus (cue), providing full or partial information about the response (response execution or withholding) to be carried out after subsequent imperative stimuli (Go and NoGo targets). The cue triggers preparatory processes that take place before the presentation of the targets and are indices of a top-down "proactive" strategy of behavioural control. Hence, on the one hand cued CPT paradigms represent robust tools for the identification of reactive inhibitory processing after NoGo target presentation during the "response phase" [30]. On the other hand, they also allow studying the allocation of cognitive resources during the silent "foreperiod" or "delay" (i.e., the cue-target interval), resulting in response preparation and in proactive inhibition.

The electroencephalographic event-related potentials (ERPs) technique represents an ideal tool to investigate proactive and reactive control processes during cued Go/NoGo tasks, due to its high temporal resolution, permitting to delineate the time course of the cognitive processes involved.

ERPs are small phasic voltage fluctuations in response to sensory, cognitive or motor events. ERPs are obtained by averaging several EEG segments of interest (epochs), time-locked to the repeated presentation of stimuli or events of interest. Epochs averaging is considered fundamental for increasing the signal-to-noise ratio, since it allows the attenuation of random noise activity, not time-locked to the event of interest. The electrophysiological response obtained is a waveform, showing changes in voltage over time that are reliably related with the event of interest. ERPs recorded at the scalp reflect the summation of excitatory and inhibitory postsynaptic potentials, produced by the synchronous activation of large population of similarly oriented cortical pyramidal neurons during information processing [31]. ERPs

associated with a given experimental stimulus or response have different advantages over both behavioural and hemodynamic measures, like fMRI and Positron Emission Tomography (PET). Compared to fMRI and PET, ERP technique has higher temporal resolution (in the order of the millisecond), but its main limitation is the low spatial resolution. Moreover, ERP technique can provide an online measure of cerebral activity even during covert processing, when there is no overt behavioural performance that can be evaluated.

In EEG studies using the Go/NoGo task, two NoGo-related ERPs have been interpreted as electrophysiological markers of reactive inhibition. The first one is the NoGo-N2, a negative deflection with larger amplitude during NoGo relative to Go trials, with a frontocentral scalp distribution and a latency of 200-400 ms post-stimulus onset [32]. The second one is the NoGo-P3, an enhanced positive deflection with maximum at Fz and Cz in NoGo relative to Go trials [30, 33] and a latency of 300-500 ms post-stimulus onset. The more anterior frontocentral distribution of NoGo-P3, with respect to the parietal maxima of the Go-P3, represents the so-called “NoGo anteriorization” effect [30, 33].

Nevertheless, the functional meaning of these ERPs is still debated. Indeed, N2 and P3 components are elicited in a broad variety of experimental paradigms testing different cognitive functions, including but not limited to motor inhibition. It has been proposed that the visual N2-like potentials are made up of three different subcomponents [34]. The first one is an anterior deviance/novelty-related N2, automatically elicited by deviant stimuli and related to the detection of perceptual mismatch, independently from cognitive control. The second subcomponent is an anterior control-related N2, associated with cognitive functions (including response inhibition, response conflict and error monitoring). The third subcomponent is a posterior N2 potential, related to attentional processes in the visual modality. The inhibitory NoGo-N2 would pertain specifically to the class of anterior control-related N2s, which are also elicited in different paradigms tapping cognitive control functions

such as the Stroop or flanker tasks. In this regard, it has been suggested that NoGo-N2 could better reflect a process of conflict monitoring between incompatible task responses for the focusing of top-down attentional control [35], rather than inhibition. According to the conflict monitoring hypothesis, in NoGo trials "conflict" occurs because the correct inhibitory response has to override the prepared prepotent Go response tendency [35]. Hence, the NoGo-N2 would represent one of the frontomedial negativities generated from a midcingulate source during the monitoring or recognition of concurrent activation of incompatible stimulus or response representations [36]. Alternatively, it has been suggested that NoGo-N2 reflects an early nonmotoric stage of inhibition [37], or the recognition of the need of inhibition (the "red flag hypothesis") [38].

Regarding the P3 component, it is evoked in a variety of different paradigms and at least two subcomponents can be differentiated [39]. The first class of subcomponents are frontal P3 potentials, including distracter-related P3a (occurring whether a stimulus is attended or not and after task-irrelevant infrequent stimuli), novelty-related P3 (elicited by deviant attended stimuli) and the NoGo-P3. These components would represent variants of the same generative P3a, related to frontal lobe activation associated with the attentional processing of stimuli. The second subcomponents is a centroparietal P3b (or classic P3), associated with updating processes in working memory and related to temporoparietal generators [39]. According to this "context-updating theory" [39], initial sensory and attentional processes of stimulus evaluation would be reflected in frontal lobe activation, leading to P3a generation. Deviations from expectations or task demands would trigger the updating of stimulus representations, engaging temporoparietal regions generating the P3b. Additionally, during the transmission of information from frontal areas to temporoparietal areas, the P3b effect would also index the inhibition of concomitant irrelevant brain processes, potentially interfering with the updating of task-relevant information. Regarding the criticism about the inhibitory meaning of the

NoGo-P3, this ERP is considered too late to reflect an ongoing inhibitory operation, peaking at or even after the overt response [37]. Alternatively, it has been associated with an evaluative processing of the outcome of inhibition or with the reset or closure of a preceding inhibitory mechanism, reflected in the NoGo-N2 [37].

Another main problem for the inhibitory interpretation of the NoGo-P3 is the possibility that this large anterior positivity of could result from the absence of a negative movement-related potential, adding at anterior recordings to the Go-P3 in case of overt responding [38, 40]. Assuming a negative movement-related potential in Go trials, which is absent on NoGo trials, the NoGo-ERP should be less negative than the Go-ERP at central electrodes about at the time of the "Go" motor response. Indeed, the topography of the P3 Go/NoGo effect, with maximum at central and frontal sites and being larger contralateral to the responding hand, shows great similarity to the topography of the negative peak of the movement-related potential. Moreover, preparatory movement-preceding negativities are supposed to be present in both Go and NoGo trials, but possibly with different time courses. Indeed, the topography of the P3 Go/NoGo effect is similar to the topography of the preceding motor-related contingent negative variation (CNV). This similarity has been explained by a continuation of the CNV during Go-P3 and/or by an overlap of the positive-going resolution of CNV to the NoGo-P3, thereby accounting for its anterior topography [41]. Hence, the resolution of the CNV in NoGo trials, which would be conversely maintained in Go trials, would result in this latter case in larger negative amplitude [38, 40]. Nevertheless, the presence of an enhanced NoGo-P3 amplitude for both motor and nonmotor (cognitive) response inhibition [e.g., 42] suggests that motor-related potentials cannot entirely account for the Go/NoGo P3 effect, and the contribution of overlapping motor-related potential remains controversial. These previous findings underline the fact that in cue-target protocols ERP waveforms evoked by the cue and the target could overlap, especially when these two stimuli are presented within short delays,

and hence they are often difficult to identify and to disentangle. Hence, investigating the effects of a warning signal on the processing of a subsequent target remains highly challenging, when studying ERP as “waveforms”.

Moreover, multiple parallel operations are engaged during the NoGo-N2 and NoGo-P3 time windows [43, 44], since the Go/NoGo task requires not only inhibition but also decision making, response selection and planning. This could explain the conflicting results regarding functional meaning and source generators of the NoGo-N2 and NoGo-P3 waves, as well as the large number of cerebral regions shown by fMRI studies of Go/NoGo task [for reviews, see 27, 45]. Dominant sources for the NoGo-N2 have been localized in bilateral prefrontal cortex [46], in the anterior cingulate cortex (ACC) [35], in right VLPFC and DLPFC [47]. Generators of the NoGo-P3 were reported in the right frontal lobe [48], but also in orbitofrontal cortex [49], in ACC and left premotor cortex [46]. Probably, many of the several brain regions reported in both EEG source analysis and fMRI studies of Go/NoGo tasks [27, 45], are not involved directly in inhibitory commands, but rather in such concomitant cognitive processes. Of note, fMRI could not well describe the exact timeline of activations and the dynamic interaction between different brain areas in real time, due to its low temporal resolution [50]. Furthermore, most of Go/NoGo ERP studies used a traditional waveform analysis that introduces a degree of experimental bias, related to the a priori selection of scalp sites and time periods to optimally evaluate the predefined ERP components of interest. Additionally, ERP waveform analysis could not accurately reflect and define temporally overlapping activities of the different neural subsystems involved in ERP generation.

In cued versions of visual CPT, various ERP components with different cortical localizations are elicited during the foreperiod, thought to represent electrophysiological markers of cue processing and maintenance, attentional resource allocation, target expectancy and motor response preparation [51, 52]. The ERP response evoked by warning stimuli is marked by an

early positivity with a maximum at frontocentral sites (P2), followed by a second positivity with a centroparietal maximum (P3a) and then by a prolonged, broadly distributed CNV across frontal, central and parietal electrodes. In this regard, previous EEG literature focused principally on late preparatory slow brain potentials, thought to index either preparation before overt or covert responses to the target, either target anticipation and expectancy. These components appear as slowly rising negative deflections between a warning cue (S1) and an imperative target stimulus (S2), which begin to emerge at least 500 ms after cue onset and last for several seconds, usually reaching their peak amplitude at the presentation of S2 [for reviews, see 53, 54]. In particular, S1-S2 cued paradigms typically elicit the so-called "CNV", a sustained negative deflection that develops after a cue signalling information on how to respond, and before an imperative target requiring an overt or covert response [55]. The CNV has a wide scalp distribution, with highest amplitude at the frontal and central electrodes. Paradigms with long cue-target interval allowed distinguishing two CNV subcomponents, namely the early and late CNV [53, 54]. The early CNV has a frontocentral topography, peaking at Cz about 400-800 ms after warning stimulus onset and it is thought to be related to the properties of S1. The early CNV reflects an orienting response to the cue and, accordingly, it has been called “orienting-wave” [56]. Furthermore, it has been associated with the evaluation or categorical description of the cue, varying as a function of its modality or intensity [e.g., 57, 58]. On the contrary, the late CNV, peaking few hundred ms before the target stimulus, has a centroparietal scalp distribution and is thought to be related to both target anticipation (and accordingly called “expectancy-wave”) and/or response preparation. Hence, it seems to reflect a combination of a movement-preceding negativity and of a stimulus-preceding negativity (SPN). The SPNs are a class of slow negative components with different scalp topographies and progressive amplitude increase, rising up before the presentation of behaviourally relevant stimuli or informative feedback signals, regardless of

whether a response is required after the stimulus. Since the SPNs do not reflect a motor response preparation, a SPN-like component contributing to the late CNV, would reflect the anticipation of the upcoming stimulus [53, 54].

Additionally, in its distribution and morphology [59] the late CNV resemble the so-called "Bereitschaftspotential" (BP) or "readiness potential" (RP), a slow negative component recorded for self-paced (i.e., voluntary, endogenously triggered) movements [60]. This slow wave begins around 1200-1500 ms prior to the self-paced movement and increases slowly in amplitude up to the movement onset. It is composed of two components, an early BP (BP1) and a late BP (BP2). The BP1 arises predominantly from the pre-SMA and SMA proper, and thereafter in the lateral premotor cortices bilaterally with possible contributions from cingulate and prefrontal cortex: it would represent a nonspecific preparation for movement, such as facilitation of cortical and subcortical motor pathways. The BP2 begins in the last 500 ms prior to movement and is generated by both SMA proper and the contralateral M1 and premotor cortex: it likely represents the selection of appropriate muscles for activation [for reviews, see 61, 62]. Of note, BP develops also before imagined movements, with an early phase not different from that recorded during actual movement and a late phase that, contrarily, does not show lateralization during imagined movements [63]. Although previous studies showed differences between cerebral activities preceding self-paced and externally triggered movements at cortical and subcortical level [e.g., 64, 65], the main cortical generator of both the BP and the late CNV are in the mesial frontal cortex, encompassing the SMA and the underlying cingulate motor areas [65-67]. However, when the cue conveys specific information about the features of the target, additional posterior sensory and frontoparietal networks, including the DLPFC, may contribute to the CNV. In particular, EEG source localization studies showed the activation of the SMA, cingulate cortex, M1 and prefrontal cortex (Broadmann Areas, BAs, 45 and 9) during the late CNV, as well as activities

in posterior occipital and parietal areas [66, 67]. Hence, the precise relationship between the late CNV and the BP remains controversial, and it is likely that the late CNV contains elements related not only to motor readiness, but also to stimulus anticipation [54, 59]. Source for the early CNV was found bilaterally in the SMA and ACC and in the middle frontal cortex (BA 9), contralateral to the motor response side, as well as in occipitotemporal cortex (BA 37) [66].

Although late preparatory slow wave potentials, indexing target anticipation and response preparation, were the main target of previous research, other earlier cue-related ERPs reflecting sensory processing of and orienting of attention to the warning signal, could play a pivotal role in the successful outcome of subsequent Go or NoGo responses. Previous EEG studies focused in particular on cue-locked P2 and P3. The P2 component, peaking at frontal site around at 150-250 ms post stimulus onset, likely correspond to another cue-related component, which was studied by comparing the cue to the distractors, the frontal selection potential (FSP) [68]. This latter ERP is a positive deflection starting around 150-200 ms, reflecting the discrimination of task-relevant stimuli from other stimuli [52]. These early cue-related frontal positivities, occurring between 180 and 300 ms, largest over prefrontal recording sites, and enhanced by task-relevant stimuli, are thought to reflect stimulus evaluation, discrimination of relevant stimuli, the selection of such stimuli for further processing and the suppression of irrelevant processing in the allocation of visual attention. Hence, these cue-related components were proposed as a correlate of sensitivity (i.e., the perceptual ability to discriminate among behaviourally relevant and non-relevant stimuli) [52, 69, 70]. After the P2/FSP, further attentional orienting and encoding of task-relevant cue would be reflected in three related potentials, namely the cue-P3, the early CNV and a posterior slow positivity with a peak latency between them [71]. The centroparietal cue-P3, peaking between 300 and 600 ms after the cue onset, is proposed as a correlate of attentional

orienting to targets and of further cue evaluation and categorization [69, 72, 73]. As discussed above, in a later phase of the foreperiod, the early frontal CNV peaking at Cz between 400-800 ms after the cue onset seems to reflect orienting to the task-relevant cue and additional processing or evaluation of information that it conveys.

Of note, the possible involvement of some specific foreperiod component in proactive inhibition has been largely overlooked. In this regard, a previous EEG study has underlined that the effect of the cue signal in reaction-time paradigms entails not only bottom-up attentional and motor preparatory processing, but also concomitant top-down inhibitory mechanisms preventing automatic wrong responses to the cue itself. This particular type of top-down, proactive inhibition during the foreperiod, would be reflected in the presence of an early cue-elicited N2 component over right frontocentral electrodes, with a latency around 320 ms after cue onset. This ERP would index a baseline gating mechanism during conditions of uncertainty that locks the initiation of a motor response before any stimulus is presented [70]. This evidence prompts further research focused on early, cue-elicited preparatory activities, which could reflect top-down proactive inhibitory mechanisms.

1.3 Motor inhibition and covert actions

Studies on proactive and reactive inhibitory mechanisms focused principally on tasks requiring the effective performance of the Go response, which represents an “overt” action execution (AE). Nevertheless, according to the “motor simulation theory” proposed by Marc Jeannerod [74], common neural substrates underlie both executed actions (“overt actions”) and potential motor acts (“covert actions”), like motor imagery (MI). Moreover, according to this view, both AE and MI could involve a covert stage during which the action is prepared, irrespective of whether the movement is subsequently performed or conversely it remains

"potential". The notion of shared neural substrates for overt and covert actions was strongly supported by the discovery of the so-called "mirror neurons" in ventral premotor cortex (vPMC) and IPL of monkeys [75, 76], and of the putative equivalent "mirror system" in humans [77, 78].

MI is the conscious, voluntary mental rehearsal of action representations without any overt movement [79]. Supporting the "motor simulation" hypothesis, a growing body of evidence underlines that AE and MI share commonalities in terms of performance as well as of underlying neural substrates [for reviews, see 74, 80]. Evidence from mental chronometry showed that the duration of imagined movements is similar to executed movements; furthermore MI also seems to follow Fitts' law stating that movement time increases with increasing task difficulty [for reviews, see 80-82]. In addition, during MI changes in autonomic function similar to those present during AE, including increases in heart and respiratory rates as well as in end-tidal PCO2 has been shown [83, 84]. Human functional neuroimaging studies revealed during MI and AE a substantial, even if incomplete, overlap of active motor-related brain regions, including frontal premotor, parietal and subcortical regions, principally including the SMA, the dPMC, the supramarginal gyrus and the SPL [85-87].

Furthermore, various EEG studies showed similar neural activities between MI and AE concerning motor aspects of action preparation. In this regard, previous research assessed principally the slow motor-related potentials. During the late stage of the foreperiod in cued paradigms, motor preparation indexed by the motor-related potentials (such as the RP and the derived lateralized readiness potential, LPR, which is the mean of the differences between contra and ipsilateral electrode sites for left- and right-hand responses) is evoked also before an imagined movement. Nonetheless, such ERPs show lower amplitudes for MI, suggesting a reduced involvement in M1 [63, 88-91]. Furthermore, it has been shown that late preparatory

motor potentials for both AE and MI are affected by variation of task parameters and are sensitive to the amount of information and to the level of ambiguity provided by the cue [92, 93].

Most of EEG studies comparing preparatory mechanisms during AE and MI, focused on late motor-related slow potentials, while data regarding early cue-related ERPs associated with stimulus processing and stimulus-response mapping are limited. Nonetheless, a recent study showed that commonalities in the preparatory phase of MI and AE are not only restricted to the motor aspects of the task, but are also present in "cognitive" processes related to attentional resources allocation, as indexed by the anterior directing attention negativity (ADAN) and late directing attention positivity (LDAP). These early, lateralized ERPs reflect cognitive attentional shifts, during unilateral manual overt response preparation. Similar ADAN and LDAP emerged for both overt executed and imagined actions when the cue was completely informative about the requested incoming movement. Dipole analysis for these potentials confirmed shared generators between imagination and execution, with ADAN activity localized in lateral premotor areas, and LDAP activity in the occipitotemporal region [92].

Nevertheless, at present, evidence for other early cognitive mechanisms preactivated before an incoming covert actions are lacking. In particular, whether and to which extent proactive inhibitory mechanisms are implemented during the early preparation for "covert actions" has never been investigated in EEG studies.

Given this converging evidence for a shared set of cerebral regions involved in encoding actions, whether or not those actions are effectively executed [74, 80, 85-87], an unsolved problem is the identification of the neural mechanisms of motor inhibition during MI. Indeed, inhibitory mechanisms are requested in order to prevent such covert action from being performed and, consequently, allowing it to remain "potential", without overt movements, in

spite of the activation of the motor system. Theoretically, motor inhibitory mechanisms during covert actions could act at two levels. The first is at the cortical level, preventing the motor programs elaborated within the parietopremotor circuits from activating M1. The second level of action of possible inhibitory mechanism is in the spinal cord: inhibitory mechanisms could act on the descending motor command before it reaches the motoneuronal level, through inhibitory or disfacilitatory influences at the spinal level [74, 94]. Different premotor areas could play a role in both these mechanisms. Indeed, the pre-SMA and the rIFG, part of a crucial motor inhibitory network together with the BG [3], could generate downstream inhibitory effects on facilitatory thalamocortical output directed to M1. Furthermore, premotor areas as vPMC in the IFG and dPMC could play a relevant role in the control of spinal circuits, by means of their spinal projections, direct or indirect through the brainstem [95]. At the same time, these areas could also act at a cortical level through direct connections with M1, exerting suppression of its excitatory output.

Sparse evidence in the literature points to the inhibitory involvement of premotor areas during different types of covert actions, namely during MI and action observation (AO) (for a taxonomic classification of covert actions, see [74]). Human fMRI studies assessing connectivity between brain regions within the motor system, provided evidence that the mesial premotor cortex (in both pre-SMA and SMA proper regions) exerts suppressive influence over M1 during MI [96, 97]. Furthermore, in monkeys an enhanced metabolic activity in rostral dPMC (absent during AE) and in M1 (at 50% level with respect to AE) have been proved during AO [98]. Of note, these latter activations paralleled a reduction of cervical spinal metabolic activity in segments containing arm motoneurons [99]. Taken together, these findings suggested a possible inhibitory mechanism trigged by the dPMC through its spinal projections, determining disfacilitation of spinal cord motoneurons. More recently, “inhibitory” mirror neurons, reducing or suppressing their basal discharge during AO, have

been demonstrated both in monkeys and in humans in ventral and mesial premotor cortex [100, 101] as well as in M1 in monkeys [102]. These data gave new insights into potential mechanisms preventing unwanted self-movements during covert actions, showing at a neuronal level how inhibitory patterns of activity could be automatically triggered during the activation of motor representations. To date, it is not known if such automatic inhibitory operations are also implemented during MI; nor it has been clarified the relationship between putative forms of "automatic" (implicit) and "voluntary" (explicit) inhibition. Of note, MI is a particular type of covert action in which the motor representation is explicitly rehearsed and concurrently implicitly inhibited. During MI, inhibitory mechanisms might be considered as automatic since, although subjects are instructed to voluntary rehearse the motor representations, they are not instructed to imagine or to put into action inhibitory commands per se. Conversely, explicit or voluntary inhibition is typically tested with the Go/NoGo or Stop-Signal tasks, in which participants are explicitly instructed to refrain from responding when presented with a specific inhibitory signal. In this case, response inhibition is voluntary and is based on top-down control mechanisms triggered when the specific stimuli are recognized. However, even if motor inhibition during MI is enacted independently from volitional effort, it could be included in an overall goal-oriented and actively chosen "covert performance modality", as individuals know that they will not overtly move during an imagined action. Evidence in this direction emerged in an EEG study, showing that cerebral activities for overt and imagined movements were already different at a very early stage of motor selection and planning. Stimulus-locked ERPs within the first 150 ms after target signals, requiring overt or covert movement execution, were dissimilar in AE and MI. These findings suggested that the prior "action intention" (overt vs. covert) could induce a different intrinsic functional organization of sensorimotor networks, leading to different sensory

processing of the stimulus, stimulus-response mapping and action-selection process for overt and covert movements [103].

To date, many questions remain open. How is the inhibition of motor commands implicitly implemented during MI? What is the relationship between putative forms of implicit, automatic and explicit, volitional inhibition? Is inhibition of covert movements during MI based on mechanisms similar to those for controlled inhibition of overt responses elicited by inhibitory signals? Finally, whether and to which extent cognitive proactive inhibitory mechanisms could contribute to the intrinsic covert nature of imagined movements is still unknown.

Chapter 2

Experimental study: overview

2.1 Aims of the study

Taking into account this background, we performed a high-density EEG study evaluating proactive and reactive cerebral processes and their related sources elicited during two types of cued Go/NoGo task, requiring the execution or withholding of an overt (Go) or a covert (MI) action, respectively.

The analyses of the EEG data were organized and conducted in two steps, with different aims:

1) Experimental Study Part 1: the first part of the study includes the analysis of the "response phase" of the cued overt and covert Go/NoGo tasks, focusing on cerebral activities time-locked to the target imperative Go or NoGo signals, for the evaluation of reactive inhibitory control of overt and covert actions. The preliminary assumption of our study was that the MI task would elicit not only explicitly evoked motor representations but also simultaneous implicit motor inhibition, possibly similar to those voluntarily implemented in NoGo trials, and presumably overlapping with NoGo-N2 and/or NoGo-P3 latency time ranges reported in the literature. In particular, we aimed at assessing: a) the presence of putative motor inhibitory mechanisms during the MI enactment; b) their underlying cerebral sources; c) their differences or similarities with respect to cerebral networks underpinning inhibition during the overt Go/NoGo task.

The Experimental Study Part 1 appears in: "Angelini M, Calbi M, Ferrari A, Sbriscia-Fioretti B, Franca M, Gallese V, Umiltà MA. Motor inhibition during overt and covert actions: an electrical neuroimaging study. PLoS One. 2015; 10:e0126800".

2) Experimental Study Part 2: the second part of the study includes the analysis of the "preparatory phase" of the cued overt and covert Go/NoGo EEG datasets, focusing on cerebral activities time-locked to the preparatory signals, for the evaluation of proactive inhibitory mechanisms of overt and covert actions and their related neural sources. We aimed at investigating whether the overt and covert modalities of the possible incoming motor response, instructed by the preparatory cue, predisposed *ab initio* a different organization of the parietofrontal areas involved with sensorimotor transformations and motor inhibitory control.

The Experimental Study Part 2 is a part of an article, which has been submitted for publication and at present, is under revision (Angelini M, Calbi M, Ferrari A, Sbriscia-Fioretti B, Franca M, Gallese V, Umiltà MA. Proactive control strategies for overt and covert Go/NoGo tasks: an electrical neuroimaging study).

Taking into account the controversies and uneven results concerning the inhibitory meaning of specific ERP waveforms components and related neural generators, which emerged from previous Go/NoGo functional neuroimaging and EEG studies (see "1.2 Electrophysiological indexes of response inhibition"), the EEG analyses of the present study are based on a spatiotemporal analysis of the scalp electric fields. This approach avoids methodological limitations of the "canonical" analysis of EEG and ERP data, based upon waveform morphology of recordings at certain electrode positions. Traditionally, ERP components are described in terms of waveform features, namely as a set of positive and negative deflections at specific latencies and electrodes. The canonical analysis of ERP waveform evaluates amplitude and latency of peaks of these weaves, assessing their sensitivity to experimental variables [104]. This approach shows different pitfalls and limitation. For instance, the *a priori* selection of time periods or components of interest recorded at a chosen subset of electrodes, leads to the possibility that other time periods or electrode locations with

significant modulations could be ignored, such as during periods of low amplitude in a given waveform. In addition, the waveform morphology and latency and the electrodes at which significant differences are present between conditions, strongly depends on the position of the reference electrode of the recording electrode. Hence, the obtained waveform shape and eventual statistical results only apply for that chosen reference [105]. Finally, with multichannel high-density ERP recording systems, different electrodes could show distinct ERP components at the same latency. In this case, it is difficult to state whether different generators underpin ERP waveforms with identical latencies but peaking at different electrodes with opposite polarity, or whether these ERPs just reflect the opposite poles of the volume-conducted activity of one dipole source. In order to avoid these confounding factors, usually ERP analyses focus on selected electrodes and latencies that possibly best define the component of interest, basing on previous literature. Nonetheless, this preselection approach does not take advantage of the full information that high-density EEG recordings can provide.

Differently from this canonical ERP approach, **t**he spatiotemporal analysis of scalp electric fields describes ERPs as a sequence of evoked electric field maps, considering the spatial properties and the temporal dynamics of scalp electric fields. This method avoids any *a priori* bias on preselected time periods or scalp locations. Another advantage of this method is its complete reference-independence: the recording reference does not influence the topography of the scalp electric field and thus does not influence global topographic measures [105]. Moreover, topographic differences in time, between experimental conditions, or under specific pathological circumstances have direct neurophysiologic interpretability. Indeed, different topographies of the electric field at the scalp can only be caused by changes in the configuration of the underlying intracranial generators [106] (although the converse is not necessarily true, since different generator configurations can lead to the same scalp fields).

Hence, this approach provides an objective means to assess reliably different cerebral networks that generate different recorded fields on the scalp [105, 107].

In the “Experimental Study Part 1” (analysis of the response phase), we performed a spatiotemporal analysis of the scalp electric field using the “microstates segmentation approach”. This approach summarizes ERP data in a sequence of time periods of stable scalp topography (segmentation maps) thought to represent “functional microstates” of the brain (i.e., discrete computational steps during information processing) (see “3.1 EEG analysis methods” for further details).

In the “Experimental Study Part 2” (analysis of the preparatory phase), we applied nonparametric randomization statistic on two parameters describing the scalp global electric field: a) the Global Field Power (GFP), for the assessment of modulations in electric field strength; b) the Global Map Dissimilarity (DISS), for the assessment of modulations in electric field topography (see “4.1 EEG analysis methods” for further details). This spatiotemporal approach allows one to distinguish whether simple modulation in response strength or, conversely, dissimilar scalp electric field topographies underpin different elicited EEG activities between experimental conditions.

Both these spatiotemporal approaches provide an objective definition of time windows for source analysis, relying on the statistical proof that the electric fields are different and thus generated by different neural sources [105, 107].

In the present thesis, the description of the experimental study will be organized as follow: the overall "Materials and Methods" (including study population, experimental paradigm, EEG recording and preprocessing, EMG recording and analysis, and MI assessment) are detailed in the following section of this Chapter. Specific spatiotemporal methods of EEG analyses, results and discussion of the Experimental Study Part 1 (analysis of the response phase) and Part 2 (analysis of the preparatory phase) are reported in Chapter 3 and Chapter 4,

respectively. Finally, general discussion of the results and conclusions are reported in Chapter 5.

2.2 Materials and Methods

2.2.1 Participants

Fifteen young adult volunteers took part in the study: nine male, six female; mean age 24.4 years (standard deviation, *SD* = 3.81); age range: 20-35 years. All participants had normal or corrected-to-normal visual acuity, no history of psychiatric or neurological impairments and were right-handed, as assessed by the Edinburgh Handedness Inventory [108]. All participants provided a written informed consent to participate in the study, which has been approved by the local ethical committee (Comitato Etico per Parma) and has been conducted according to the principles expressed in the Declaration of Helsinki.

2.2.2 Experimental Paradigm

The experimental paradigm was a modified form of a cued O-X CPT already used in previous Go/NoGo studies [30, 33, 48, 109]. From the initial development paradigms [29], several CPT versions have been extensively used to assess executive functions, in particular sustained and selective attention and response inhibition [28, 30, 33, 48, 109]. In cued forms of CPT, interspersed among a large number of distractors, a warning signal (cue) precedes imperative signals (targets) that require the execution (Go condition) or the withholding (NoGo condition) of a motor response. Hence, cued forms of CPT are suitable for the evaluation of the cognitive control of the motor system, requiring at target onset a decision-making process between executing or refraining from an anticipated motor response (for a comparison between the CPT and Go/NoGo task, see [110]). In particular, the cued O-X CPT, similar to

that used in the current study, has been proved a powerful tool to investigate motor inhibitory control [30, 33, 48, 109].

Our paradigm consisted of four experimental conditions organized in two blocks (sessions A, B) (Figure 1): overt Go and NoGo conditions were presented in session A (overt Go/NoGo task); MI and NoGo Motor Imagery (NoGoMI) conditions were tested in session B (covert Go/NoGo task). We separated the four conditions in two blocks in order to maintain a clear distinction between the inhibitory mechanism in NoGo condition and the putative motor inhibition in MI condition, and to avoid potentially confounding interferences leading to difficult interpretations of the results. The order of presentation of the two sessions was balanced among participants.

Stimuli consisted of 12 different white letters (*A*-*H*, *J*, *L*, *O* and *X*) on a black background, sequentially presented in pseudo-random order at the center of a 19-inches computer screen positioned at 60 cm from participants. The letters on the screen were 20 mm high and 15 mm wide, resulting in a visual angle of 1.91° vertically and 1.43° horizontally. The same letter was never immediately repeated. Each letter was presented for 200 ms and separated from the next one by a black screen whose duration varied randomly between 1650 and 2000 ms.

In both sessions (Figure 1) the letter “O” was the preparatory cue, representing a warning signal to prepare to respond. It was followed by the imperative target stimulus, which specified the requested response. Hence, each trial of the four conditions consisted in a preparatory phase (between the onset of the cue letter “O” and the onset of the successive target stimulus) and in a response phase (between target onset and the onset of the successive letter).

In session A (Figure 1) the letter “X” after the “O” cue represented the target stimulus for Go condition. It required the overt execution of a motor response, consisting in pressing a button on a pad, positioned in front of the participants, with the index finger of the right hand. In

session B (Figure 1) the letter "X" after the "O" cue represented the target stimulus for the MI condition, requesting the participants to perform a kinaesthetic MI of the button-press movement (i.e., to imagine themselves pressing the button in a first-person perspective). In both sessions the other letters (*A-H, J, L*) required response inhibition if they were preceded by an "O", representing target stimuli in session A for NoGo and in session B for NoGoMI conditions, respectively; if not preceded by an "O", they served as meaningless distractors. Each of the two sessions consisted of 80 trials "O-X" (Go and MI trials, in session A and B, respectively), 80 trials "O-noX" (NoGo and NoGoMI, in session A and B, respectively) and 240 distractors. The sequence of presentation of trials and distractors was randomized. Each session lasted about 20 minutes, with a five minutes rest period between the two sessions.

Before starting the recording, participants completed a brief training phase. They were presented with a training block including two parts (A and B), whose order of presentation was balanced among participants: each part included four trials for each condition (four Go and four NoGo trials in part A; four MI and four NoGoMI trials in part B) and 16 distractors. Participants familiarized with the Go motor task (consisting in pressing a button on a pad, positioned in front of them, with the index finger of their right hand) and with the MI task. For the MI task, participants were specifically instructed to imagine themselves pressing the button in a first-person perspective, i.e., to perform a kinaesthetic MI and not only to visually imagine the movement. The instructions given for the Go/NoGo and MI/NoGoMI tasks were maintained uniform between the two sessions (i.e.: for the Go and MI conditions participants were requested to press or to imagine themselves pressing the button, respectively; for the NoGo and the NoGoMI conditions participants were requested to refrain from responding or to imagine themselves refraining from responding, respectively). For the NoGoMI condition, participants were not explicitly asked to actively think to suppress an imagined button-press

movement. Speed and accuracy in motor responses were emphasized equally during the explanation of the tasks.

Stimuli delivery and response recording were controlled with the E-prime 2.0 software; the button-press recording was used to assess omission (i.e., Go trials without responses) and commission (i.e., responses in NoGo trials) errors.

2.2.3 EEG Recording and Preprocessing

Continuous EEG was recorded using the 128-channels Geodesic EEG System (Electrical Geodesics Inc., Oregon) and the HydroCel Geodesic Sensor Net (GSN300), at a sampling rate of 500 Hz (0.01 Hz high-pass filter) with the vertex as online reference; electrodes impedances were kept below 50 kΩ. Offline analyses were performed with Cartool software (freely available at: http://brainmapping.unige.ch/cartool) [111].

The raw EEG data were band-pass filtered (1-30 Hz, notch 50 Hz) and recalculated against the average reference. The outermost belt of electrodes of the sensor net, more prone to show residual muscular artifacts, was excluded and the original template was reduced from 128 to 110 channels. Artifacted channels were interpolated using a spherical spline interpolation method implemented in Cartool software [112].

To evaluate target-elicited ERPs (analysis of the response phase), epochs from 200 ms before to 700 ms after targets onset were averaged across trials, separately for each participant and condition; these single-subject averages were then used to compute four group-averaged ERPs, one for each experimental condition.

To evaluate cue-elicited ERPs (analysis of the preparatory phase), epochs from 200 ms before to 1000 ms after “O” letter onset were averaged across trials, separately for each participant and session; these single-subject averages were used to compute two group-averaged ERPs, one for each experimental session.

Trials with erroneous responses (omission and commission errors) and NoGo, MI and NoGoMI trials with concomitant EMG activity during the response phase, as well as trials with EMG activity before target onset were excluded (see "2.2.4 EMG recording and Analysis"). The remaining trials were submitted to an automated threshold rejection criterion of 65 μV and visually inspected for detection of ocular, muscular and other artifacts. To maintain a good signal-to-noise ratio, for the response phase a lower limit of 40 artifact-free correct trials per participant per condition was set. The mean ± *SD* of accepted epochs was: for Go condition 45.3 (*SD* = 1.45); for NoGo condition 44.7 (*SD* = 2.9); for MI condition 45.1 (*SD* = 1.8); for NoGoMI condition 43.8 (*SD* = 3.6). A repeated measures ANOVA ($p < .05$), performed in order to exclude differences in the number of accepted trials among conditions, did not result significant ($F_{(3,42)} = 2$, $p > .05$). For the preparatory phase, a lower limit of 80 artifact-free correct trials per participant per session was set. The mean of accepted trials was 95.13 (*SD* = 11.2) for session A and 92.13 (*SD* = 10.2) for session B. A two-tailed *t*-test ($p < .05$) was performed in order to exclude differences in the number of accepted trials between sessions, which did not result significant ($t = 1.36$, $p > .05$).

2.2.4 EMG Recording and Analysis

Surface EMG of the right First Dorsal Interosseous (FDI) muscle was recorded with EGI's Polygraph Input Box (PIB) continuously during both experimental sessions (sampling rate 500 Hz, band-pass filter 30-200 Hz, notch 50 Hz) using bipolar derivation. A moving average (period = 300 ms), centred on each 100 ms epoch, was applied to the rectified EMG data of each participant recorded in the time interval from -200 (baseline) to 700 ms from target stimulus onset for the response phase, and from -200 (baseline) to 1000 ms from cue onset for the preparatory phase. An offset procedure was performed using as offset value the mean

baseline EMG plus its *SD* multiplied by two (baseline threshold). This latter value was compared, by means of independent samples *t* test with a significance criterion of $p < .01$, with the baseline. The aim of EMG recording was twofold. Firstly, in order to control for the possibility that differences in EEG activity among conditions could have been influenced by residual movements, NoGo, MI and NoGoMI trials with significant EMG activity (identified with the procedure described above) during the response phase, and all trials with significant EMG activity during the preparatory phase, were discarded.

Secondly, since the electrophysiological correlates of motor inhibition need to be present before the movement onset, in order to define the temporal relationship between cortical activity and the motor response, in Go trials the mean latency of the first rising phase of the EMG activity, measured with respect to the onset of the Go stimulus (Go EMG onset), was calculated.

2.2.5 Motor Imagery Assessment

After the EEG recording, the MI ability of participants was evaluated by means of the Vividness of Movement Imagery Questionnaire (VMIQ) [113]. The VMIQ consists of 24 items, each of which is a description of a common movement (e.g., walking, kicking a ball in the air). Participants were asked to imagine each item from a third-person (external imagery) and from a first-person (internal imagery) perspective: then, they rated the vividness of the imagined movement on a five-point Likert-type scale, with responses ranging from 1 (perfectly clear image) to 5 (no image at all). The rating procedure for the questionnaire is summative, with the lower score indexing a more vivid imagery. Three scores were obtained: 1) VMIQ-Other (range 24-120), for the external imagery; 2) VMIQ-Self (range 24-120), for the internal imagery; 3) VMIQ-Total (range 48-240), resulting from the addition of the other two scores.

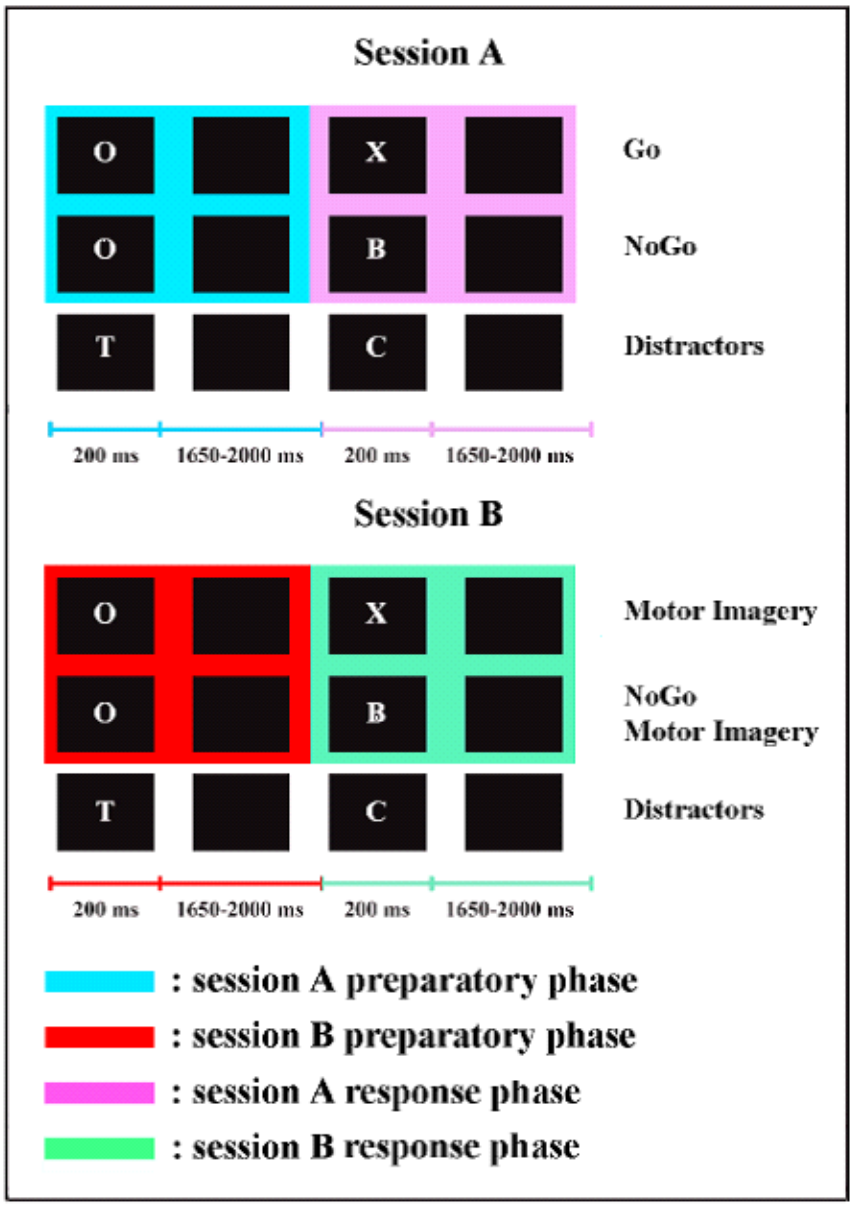

Figure 1. Experimental paradigm and stimuli.

Chapter 3

Experimental Study Part 1

Analysis of the response phase

3.1 EEG analysis methods

The EEG analyses of the "response phase" was based on a spatiotemporal analysis of the scalp electric field using the "microstates segmentation approach" [50, 114]. This approach summarizes ERP data in a sequence of time periods of stable scalp topography, called "segmentation maps", thought to represent "functional microstates" of the brain (i.e., discrete computational steps during information processing) [106]. These periods of stable scalp topography are a more objective means for defining ERP components and time windows for source analysis, relying on the statistical proof that the electric fields are different and thus generated by different neural sources.

The "microstates segmentation approach" is based on the empirical observation in both continuous EEG and ERPs that the electric field configuration (map) at the scalp does not randomly change over time, but rather remain rather stable for tens to hundreds of milliseconds (on average around 80-120 ms) [115]. Then, with brief intervening intervals of topographic instability, it rapidly changes, to remain again in a new stable configuration. Each of these periods of stable electric field configuration would represent a cerebral functional microstate during information processing [106]. Basing on this empirical observation, cerebral electric activity can be described as a sequence of subsecond time periods (electric functional microstates), which are each characterized by quasi-stable spatial distributions of electric potential and described by a distinct map topography**.** Since different electric potential

map are generated by different configuration of active cerebral sources, different microstates are thought to reflect specific functions of the brain. Hence, the reduction of EEG data to such segments of different stable scalp topographies provides a reliable means for defining specific functional activation patterns of the neuronal network implied in a given task [50, 107, 114].

The procedure for the "microstate segmentation" of ERP data entails different steps. First, in order define the optimal number of maps that best explain the whole data set and the time periods during which they appear, group-averaged ERPs are calculated for each experimental condition. Then, a statistical method based on cluster analysis is applied to the group-averaged data across experimental conditions, in order to identify the sequence of different electric field configurations (ERP template maps) that best accounts for the data and the time period during which they occur. The hypotheses generated at the group-average level are then statistically tested at the single-subject level by means of a so called "fitting procedure" based on the spatial correlation between maps obtained from the group-average ERPs and the single-subject ERP data [105, 111 105]. The fitting procedure allows assessing the goodness of this fit and the duration, onset and offset of each of these maps in a given condition in each subject. Then, statistical analysis is performed to determine the specificity of the microstates maps for different experimental conditions, proving that they appear significantly more dominant or longer in a given condition compared to another. Hence, source localization applied to these segmentation maps is based on the statistical proof that the electric fields were different, and thus generated by different source configurations.

3.1.1 EEG Microstate Analysis

The first 700 ms post-target period, containing NoGo-N2 and NoGo-P3 ERPs described in literature [45], were analysed in terms of the spatiotemporal characteristics of the global electric field on the scalp [105, 111, 114]. A pattern analysis of the ERP scalp topography

based on a modified hierarchical clustering algorithm termed “Atomize and Agglomerate Hierarchical Clustering” [105] was performed on the group-averaged ERPs, in order to summarize data by a limited number of scalp potential fields (“segmentation maps” or “microstates”), and to identify their sequence over time within a given dataset. This cluster analysis is reference-free and insensitive to pure amplitude modulation of the same scalp potential field across conditions, since normalized maps are compared. It was performed across time and experimental conditions separately for the two sessions: one segmentation procedure was applied on Go and NoGo conditions data, and another one on MI and NoGoMI data. A temporal criterion of a minimal duration of a given map in the group-averaged data for at least 10 consecutive data points (20 ms at our 500 Hz sampling rate) was applied [111]. The optimal number of maps (i.e., the minimal number of maps accounting for the greatest variance of the dataset) was assessed by a modified Krzanowski-Lai criterion [105, 116].

To verify statistically the validity of the results of the microstate analysis, we then applied a competitive fitting procedure, based on the calculation of the strength-independent spatial correlation between single-subject ERPs and each segmentation map identified in the group-averaged data [50, 105]. Each time point of the individual subject ERPs was labeled according to the selected map with which it best correlated spatially: for each participant and condition, the number of time frames assigned to one map represented the “map presence”. If different maps appeared in a given time window in the conditions, repeated measures ANOVAs ($p < .05$) were performed on the map presence data, with Condition and Map as within-subject factors. Any significant interaction was further evaluated by means of planned comparisons ($p < .05$). The cluster and fitting analyses determined whether and when different experimental conditions were more often described by one map versus another, and therefore if different neural generators better accounted for particular experimental conditions [50, 105].

3.1.2 Source Analysis

As a final step, the electrical source analysis of the segmentation maps was performed, using a distributed linear inverse solution based on a Local Auto-Regressive Average (LAURA) regularization approach [117]. LAURA model reconstructs the brain electric activity in each point of a 3D grid of solution points, selecting the source configuration that better mimics the biophysical behaviour of electric fields without a priori assumption on the number of dipoles in the brain.

According to the electromagnetic theory described in the Maxwell equations, the LAURA algorithm assumes that the strength of the source falls off (regress) with distance (namely, with the inverse of the cubic distance for vector fields, and with the inverse of the squared distance for potential fields). LAURA integrates this law as a constraint in terms of a local autoregressive average, with coefficients depending on the distances between solution points. Consequently, the activity at one point depends upon two contributions: one fixed by the biophysical laws and another determined from the data [114].

The solution space was calculated on a locally spherical head model with anatomical constraints (L-SMAC) [118] and comprised 3001 solution points (voxels) homogeneously distributed within the brain structures of the Montreal Neurological Institute (MNI152) average brain. All solution points were labelled with their Talairach and Tournoux coordinates [119] as well as their anatomical labels.

As a preliminary step, the source of each mean segmentation map was evaluated, applying the LAURA algorithm at the group-averaged ERP fields of the four conditions. This operation does not give indications about the statistical reliability of these sources at the individual level and provides only one current density maximum for each segmentation map: consequently, weak but consistent differences in other areas might be ignored due to thresholding. Hence, to statistically validate whether these distributed activations over all solution points were

significantly different among conditions, we conducted a “voxel-wise parametric mapping analysis” at individual level [114]: when different maps were present among conditions, paired *t* tests were performed for each solution point. To do that, individual ERP data were averaged over the time period of each different map, in order to generate a single data point per period for each participant and condition. Then, the LAURA current densities source estimations for each solution point were contrasted by means of paired *t* tests. These statistical comparisons were performed first between conditions in each session and then by contrasting MI with Go and with NoGo conditions data. Solution points with *p* values < .05 ($t_{(14)} > 2.14$/ < -2.14) were considered significant; in addition, a cluster threshold of at least 10 contiguous activated solution points was applied.

3.2 Results

3.2.1 Performance and EMG Recording

The mean percentage of incorrect responses ± *SD* for Go condition (omission errors) was 2.08 % ± 2.52, and for NoGo condition (commission error) was 2.25 % ± 2.72.

The mean ± *SD* Go EMG onset was 415 ± 69 ms after Go target presentation.

3.2.2 Motor Imagery Assessment

The mean VMIQ-Total score ± *SD* was 103.4 ± 25.24; the mean VMIQ-Other score ± *SD* was 52.07 ± 14.3; the mean VMIQ-Self score ± *SD* was 51.33 ± 14.52. On average, participants had “clear and reasonably vivid” external (mean score on the five-point Likert-type scale ± *SD*: 2.17 ± 1.05) and internal (mean ± *SD*: 2.14 ± 1.13) MI ability.

3.2.3 EEG Microstate Analysis

For completeness and to allow comparison of the results of microstate analysis to previous literature on Go/NoGo tasks based on ERP waveform analysis, the superimposed group-averaged (n = 15) ERP waveforms of the four conditions from selected midline electrodes, where maximum modulatory effects are expected [32-35, 37, 45], are shown in Figure 2. Of note, the typical N2 and P3 Go/NoGo effects were replicated. By visual inspection, a clear NoGo-N2 (peak at Fz, with amplitude: -2.1 μV and latency: 276 ms) and NoGo-P3 component (peak at Cz, with amplitude: 4.21 μV and latency: 382 ms) emerged.

The two topographic pattern analyses revealed a series of 12 different segmentation maps (i.e., microstates) accounting for the electric field configuration of the collective group-averaged dataset in session A (Go and NoGo conditions) (Figure 3) and nine maps for session B (MI and NoGoMI conditions) (Figure 4). These two sequences of maps explained respectively 91.89 % (session A) and 89 % (session B) of the variance in ERPs. Results for each session are presented separately.

1) Session A: Go and NoGo Conditions

For the Go condition the microstate analysis revealed a sequence of eight maps (i.e., Go.NoGo-Map 1: 0-108 ms post-target onset; Go.NoGo-Map 2: 110-140 ms; Go.NoGo-Map 3: 142-214 ms; Go-Map 4: 216-254 ms; Go-Map 6: 256-304 ms; Go-Map 7: 306-410 ms; Go-Map 9: 412-546 ms; Go-Map 12: 548-700 ms) (Figure 3 A1, A2 and B).

For the NoGo condition seven maps were detected (i.e., Go.NoGo-Map 1: 0-112 ms post-target; Go.NoGo-Map 2: 114-144 ms; Go.NoGo-Map 3: 146-220 ms; NoGo-Map 5: 222-316 ms; NoGo-Map 8: 318-432 ms; NoGo-Map 10: 434-536 ms; NoGo-Map 11: 538-700 ms) (Figure 3 B, C1 and C2).

In particular, while three maps (Go.NoGo-Maps 1, 2 and 3) were found in both conditions, different maps were observed between Go and NoGo conditions over the 216-316 ms time period (Go-Maps 4 and 6, NoGo-Map 5) and the 318-700 ms time period (Go-Maps 7, 9, 12; NoGo-Maps 8, 10, 11). These intervals correspond to the NoGo-N2 and NoGo-P3 latencies of ERP waveform components (see Figure 2).

These results were statistically validated by means of the fitting procedure (see "3.1.1 EEG Microstate Analysis"). The statistical analysis was performed separately in three time windows based on the time of occurrence of the microstates and their representative segmentation maps in the group-averaged data. For each time window, the maps found in the group-averaged data were searched in the individual participants' ERPs in each condition, and duration of each map was calculated. Since the fitting procedure implies the preselection of time windows of equal duration between conditions, results of the ANOVAs on number of time frames for the main effect of Condition were always not significant; hence they will not be reported.

In the first time window (0-220 ms), Go.NoGo-Maps 1, 2 and 3 were included in the fitting (Figure 3 A2 and C2). The 2 x 3 ANOVA did not yield significant results (main effect of Map: $F_{(2,28)} = 3.09$, $p > .05$; Condition x Map interaction: $F_{(2,28)} = 1.5$, $p > .05$) in accord with the segmentation data showing the same map sequence in the two conditions.

In the second time window (216-316 ms), Go-Maps 4, 6 and NoGo-Map 5 were included in the fitting. The 2 x 3 ANOVA showed a significant Condition x Map interaction ($F_{(2,28)} = 19.21$, $p < .0001$): this result indicated that different maps better accounted for each condition, as confirmed by planned comparisons for Go-Map 6 ($F_{(1,14)} = 19.9$, $p = .0005$) and for NoGo-Map 5 ($F_{(1,14)} = 29.36$, $p < .0001$), but not for Go-Map 4 ($F_{(1,14)} = 1.68$, $p > .05$).

In the third time window (306-700 ms), Go-Maps 7, 9, 12 and NoGo-Maps 8, 10, 11 were included in the fitting. The 2 x 6 ANOVA showed a significant main effect for Map ($F_{(5,70)} =$

5.53, $p <$ .0005), due to the different duration of the various microstates (Figure 3 A2 and C2); more importantly, Condition x Map interaction was significant ($F_{(5,70)} = 8.49$, $p <$ .0001). Planned comparisons confirmed the significant difference of map presence between conditions for all maps, except for NoGo-Map 11 (Go-Map 7: $F_{(1,14)} = 15.18$, $p < .005$; Go-Map 9: $F_{(1,14)} = 6.91$, $p < .05$; Go-Map 12: $F_{(1,14)} = 6.36$, $p < .05$; NoGo-Map 8: $F_{(1,14)} = 16.08$, $p < .005$; NoGo-Map 10: $F_{(1,14)} = 7.78$, $p < .05$; NoGo-Map 11: $F_{(1,14)} = 3.42$, $p > .05$). In summary, for all maps, except for Go-Map 4 and NoGo-Map 11, the fitting procedure confirmed at the single-subject level the segmentation results obtained at the group-averaged level for Go and NoGo conditions.

2) Session B: Motor Imagery and NoGo Motor Imagery Conditions

For the MI condition six different maps were detected (MI.NoGoMI-Map 1: 0-144 ms post-target; MI.NoGoMI-Map 2: 146-224 ms; MI-Map 3: 226-268 ms; MI-Map 5: 270-356 ms; MI.NoGoMI-Map 7: 358-500 ms; MI.NoGoMI-Map 8: 502-700 ms) (Figure 4 A1, A2 and B).

For the NoGoMI condition the microstate analysis revealed a total of seven maps (MI.NoGoMI-Map 1: 0-148 ms; MI.NoGoMI-Map 2: 150-228 ms; NoGoMI-Map 4: 230-306 ms; NoGoMI-Map 6: 308-346 ms; MI.NoGoMI-Map 7: 348-514 ms; MI.NoGoMI-Map 8: 516-644 ms; NoGoMI-Map 9: 646-700 ms) (Figure 4 B, C1 and C2).

The two conditions were characterized by the presence of different segmentation maps from 226 to 356 ms (MI-Maps 3, 5 and NoGoMI-Maps 4, 6) and from 646 to 700 ms (MI.NoGoMI-Map 8 and NoGoMI-Map 9) after target onset. The same sequence of common topographical maps appeared in both conditions in the remaining period (Figure 4).

The reliability of these microstates was assessed at the individual level by means of the fitting procedure, applied in three time windows based on the appearance of maps in group-averaged segmentation results (Figure 4 A2 and C2).

In the first time window (0-228 ms) MI.NoGoMI-Maps 1 and 2 were included in the fitting; the 2 x 2 ANOVA did not yield significant results (main effect of Map: ($F_{(1,14)} = .35$, $p > .05$; Condition x Map interaction: $F_{(1,14)} = .25$, $p > .05$), in accord with the segmentation data, showing the same map sequence in the two conditions.

In the second time window (226-356 ms) MI-Maps 3 and 5 and NoGoMI-Maps 4 and 6 were fitted. The 2 x 4 ANOVA showed a significant main effect of Map ($F_{(3,42)} = 14.56$, $p < .0001$) due to different duration of the various maps (Fig 4 A2 and C2) and, more importantly, a significant Condition x Map interaction ($F_{(3,42)} = 10.14$, $p < .0001$). Planned comparisons confirmed the significant difference of map presence between the two conditions for MI-Map 5 ($F_{(1,14)} = 11.56$, $p < .005$) and for NoGoMI-Map 4 ($F_{(1,14)} = 11.80$, $p < .005$), but not for MI-Map 3 ($F_{(1,14)} = .007$, $p > .05$) and for NoGoMI-Map 6 ($F_{(1,14)} = 3.47$, $p > .05$).

In the third time window (348-700 ms), MI.NoGoMI-Maps 7 and 8 and NoGoMI-Map 9 were included in the fitting. The 2 x 3 ANOVA showed a significant main effect for Map ($F_{(2,28)} = 10.53$, $p < .005$), due to the different duration of the maps (Figure 4), but did not show significant Condition x Map interaction ($F_{(2,28)} = 1.3$, $p > .05$), indicating that the segmentation maps did not differed between the two conditions.

In summary, for all maps, except for MI-Map 3 and NoGoMI-Maps 6 and 9, the fitting procedure confirmed at the single-subject level the segmentation results obtained at the group-averaged level for MI and NoGoMI conditions.

3.2.4 Source Analysis

The results of the group-averaged LAURA source estimations of each mean map of the four conditions are shown in Figures 3B and 4B and the Talairach and Tournoux coordinates of the current density maximum of each map are summarized in Tables 1 and 2.

Results of the voxel-wise parametric mapping analysis of the sources of the condition-specific microstates statistically confirmed by the fitting procedure will be presented. Areas with significantly different activations ($p < .05$, $t_{(14)} > 2.14$ / < -2.14; cluster threshold of 10 contiguous activated solution points) will be reported, with *t* and *p* values, Talairach and Tournoux coordinates (x,y,z) and anatomical labels of solution points with the local maximum different activities.

1) Session A: Go and NoGo Conditions

Voxel-wise paired *t* test between NoGo-Map 5 and Go-Map 6 revealed a significant higher activity in NoGo condition (Figure 5A, red) in five cortical clusters, localized in:

1) left prefrontal cortex, encompassing frontopolar cortex (BA 10) and extending toward the DLPFC in middle frontal gyrus (BA 46) ($t_{(14)} = 3.49$, $p < .005$; x,y,z: -18,63,14 mm; left superior frontal gyrus, BA 10);

2) left pre-SMA (BA 6) and underlying bilateral midcingulate cortex (MCC) (BAs 24, 32) ($t_{(14)} = 3.29$, $p < .01$; x,y,z: -11,6,51 mm; left medial frontal gyrus, BA 6);

3) left dPMC, encompassing left middle frontal and adjacent precentral gyrus (BA 6) ($t_{(14)} = 2.59$, $p < .05$; x,y,z: -26,13,58 mm; left middle frontal gyrus, BA 6);

4) right IPL (BAs 39, 40) ($t_{(14)} = 5.04$, $p < .0005$; x,y,z: 33,-53,34 mm; right IPL, BA 40);

5) left middle and superior temporal gyri (BA 22) ($t_{(14)} = 5.36$, $p = .0001$; x,y,z: -56,-32,5 mm; left middle temporal gyrus, BA 22).

Higher activity in Go as compared to NoGo condition (Figure 5A, blue) was found in left temporooccipital areas, encompassing inferior temporal and fusiform gyrus (BAs 20, 37) ($t_{(14)} = -3.59$, $p < .005$; x,y,z: -33,-33,-14 mm; left temporal fusiform gyrus, BA 20).

The voxel-wise paired *t* test comparing NoGo-Map 8 and Go-Map 7 showed a significantly higher activation in NoGo condition (Figure 5B, red) in four anterior cerebral clusters localized in:

1) left frontopolar cortex (BA 10) ($t_{(14)} = 2.75$, $p < .05$; x,y,z: -18,63,14 mm; left superior frontal gyrus, BA 10);

2) bilateral pre-SMA (BA 6) and underlying MCC, extending anteriorly in perigenual ACC (BAs 24, 32) ($t_{(14)} = 4.38$, $p < .001$; x,y,z: 3,13,44 mm; right medial frontal gyrus, BA 6);

3) left dPMC (BA 6) ($t_{(14)} = 3.28$, $p < .01$; x,y,z: -33,1,38 mm; left middle frontal gyrus, BA 6);

4) right IFG (BA 45) ($t_{(14)} = 2.71$, $p < .05$; x,y,z: 41,19,16 mm; right IFG, BA 45).

Higher activations in Go condition (Figure 5B, blue) were found in four posterior cerebral clusters localized in:

1) right IPL (BA 40) ($t_{(14)} = -3.44$, $p < .005$; x,y,z: 56,-38,33 mm; right supramarginal gyrus, BA 40);

2) left SPL (BA 7) ($t_{(14)} = -2.65$, $p < .05$; x,y,z: -18,-51,61 mm; left SPL, BA 7);

3) bilateral occipital extrastriate visual areas, including cuneus, occipital middle, inferior and lingual gyri (BA 18) ($t_{(14)} = -4.21$, $p < .001$; x,y,z: 3,-69,0 mm; right lingual gyrus, BA 18);

4) left temporooccipital areas, encompassing inferior temporal and fusiform gyri (BAs 20, 37) ($t_{(14)} = -3.08$, $p < .01$; x,y,z: -56,-12,-21 mm; left inferior temporal gyrus, BA 20).

The voxel-wise *t* test comparing NoGo-Map 10 and Go-Map 9, revealed stronger activations in NoGo condition (Figure 5C, red) in four cerebral clusters in:

1) left frontopolar cortex (BA 10) ($t_{(14)} = 3.69$, $p < .005$; x,y,z: -41,47,-5 mm; left middle frontal gyrus, BA 10);

2) left dPMC (BA 6) ($t_{(14)} = 2.89$, $p < .05$; x,y,z: -33,13,44 mm; left middle frontal gyrus, BA 6);

3) right IFG (BAs 44, 45, 47) and anterior insula (BA 13) ($t_{(14)} = 4.31$, $p < .001$; x,y,z: 41,4,10 mm; right insula, BA 13);

4) left middle temporal gyrus (BA 21) ($t_{(14)} = 2.73$, $p < .05$; x,y,z: -56,3,-9 mm; left middle temporal gyrus, BA 21).

Enhanced activity in Go condition (Figure 5C, blue) was found in two posterior cerebral clusters localized in:

1) bilateral SPL and precuneus (BA 7), extending on the right side toward postcentral gyrus (BAs 3, 5) ($t_{(14)} = -4.28$, $p < .001$; x,y,z: -11,-52,47 mm; left precuneus, BA 7);

2) bilateral occipital extrastriate visual areas in left occipital middle, inferior and lingual gyri and in right cuneus and lingual gyri (BAs 18, 19, 30) ($t_{(14)} = -3.97$, $p < .005$; x,y,z: -26,-84,1 mm; left middle occipital gyrus, BA 18).

2) Session B: Motor Imagery and NoGo Motor Imagery Conditions

In our periods of interest, the topographical and fitting analyses showed that only two microstates (MI-Map 5 and NoGoMI-Map 4) were significantly different between the two conditions (see Figure 4). The voxel-wise *t* test revealed a higher activation in MI as compared to NoGoMI (Figure 6A, red) in three frontal clusters localized in:

1) left DLPFC, including middle and inferior frontal gyri (BA 46) ($t_{(14)} = -3.14$, $p < .01$; x,y,z: -41,40,8 mm; left IFG, BA 46);

2) left pre-SMA (BA 6) ($t_{(14)} = -2.94$, $p < .05$; x,y,z: -11,6,58 mm; left medial frontal gyrus, BA 6);

3) right IFG (BAs 45, 47) ($t_{(14)} = -3.54$, $p < .005$; x,y,z: 48,18,2 mm; right IFG, BA 47).

Higher activity in NoGoMI as compared to MI (Figure 6A, blue) was found in:

1) right posterior parietal cortex (PPC), encompassing SPL and precuneus (BA 7) and IPL (BA 40) ($t_{(14)} = 4.93$, $p < .0005$; x,y,z: 41,-52,54 mm; right SPL, BA 7);

2) right occipital extrastriate visual cortex in occipital superior, middle, inferior and lingual gyri (BAs 18, 19) ($t_{(14)} = 3.72$, $p < .005$; x,y,z: 41,-83,21 mm; middle occipital gyrus, BA 19);

3) left posterior middle and superior temporal gyri (BA 39) ($t_{(14)} = 2.79$, $p < .05$; x,y,z: -41,-61,20 mm; left middle temporal gyrus, BA 39).

3) Statistical Source Comparison between Sessions A and B

In session B significant topographic differences between conditions were present between 226 and 356 ms post-target onset: this finding suggests that neural activities related to putative motor and inhibitory mechanisms during MI were likely implemented in such time window. Hence, in order to identify differences and/or similarities between supposed inhibitory mechanisms activated during MI and NoGo conditions, we compared MI-Map 5 with microstates evidenced in session A conditions during an overlapping time-period, namely Go-Map 6 and NoGo-Map 5 (Figures 3 and 4).

A voxel-wise paired *t* test between MI-Map 5 and Go-Map 6 revealed significant higher activity in MI with respect to Go condition (Figure 6B, red) in 4 cerebral clusters localized in:

1) left dPMC encompassing left middle frontal and precentral gyri (BA 6) ($t_{(14)} = 4.22$, $p < .001$; x,y,z: -48,-1,45 mm; left precentral gyrus, BA 6);

2) right IFG (BAs 44, 45, 47) ($t_{(14)} = 2.97$, $p < .05$; x,y,z: 56,32,-4 mm; right IFG, BA 47);

3) left middle and superior temporal gyri (BA 22) ($t_{(14)} = 3.69$, $p < .005$; x,y,z: -48,-40,5 mm; left middle temporal gyrus, BA 22);

4) right anterior middle temporal gyrus (BA 21) and temporopolar cortex (BA 38) ($t_{(14)}$ = 3.52, p < .005; x,y,z: 56,2,-22 mm, right middle temporal gyrus, BA 21).

A voxel-wise *t*-test comparing MI-Map 5 and NoGo-Map 5 revealed a higher activity in MI (Figure 6C, red) in two cerebral clusters in:

1) right IFG (BAs 45, 47) ($t_{(14)}$ = 3.96, p < .005; x,y,z: 56,32,-4 mm; right IFG, BA 47);

2) left temporooccipital areas encompassing inferior temporal and fusiform gyri (BAs 20, 37) ($t_{(14)}$ = 6.76, p < .0001; x,y,z: -26,-48,-7 mm; left fusiform gyrus, BA 37).

Higher activity in NoGo condition with respect to MI condition (Figure 6C, blue) was found in:

1) left frontopolar cortex (BA 10) ($t_{(14)}$ = -3.46, p < .005; x,y,z: -18,47,-5 mm; left medial frontal gyrus, BA 10);

2) bilateral MCC (BAs 32, 24) ($t_{(14)}$ = -4.4, p < .001; x,y,z: 11,19,30 mm; right cingulate gyrus, BA 32);

3) right PPC, encompassing both SPL (BA 7) and IPL (BA 40), extending toward post-central gyrus (BAs 3, 5) ($t_{(14)}$ = -4.92, p < .0005; x,y,z: 26,-45,54 mm; right SPL, BA 7);

4) right posterior middle temporal gyrus (BAs 21, 37) ($t_{(14)}$ = -2.49, p < .05; x,y,z: 56,-62,0 mm; right middle temporal gyrus, BA 37).

3.3 Discussion

The principal aim of the Experimental Study Part 1 was to evaluate putative inhibitory mechanisms activated during the covert action of MI, and to compare them with inhibitory mechanisms of overt actions elicited during an overt NoGo condition. The segmentation analyses revealed the presence of different cerebral microstates, indexing different neural processing and generators [106], both in NoGo with respect to Go, and in MI with respect to NoGoMI conditions. Of note, a different temporal distribution of these condition-specific

neural activations emerged in the two sessions (Figures 3 and 4). In session A, a sequence of statistically significant microstates different between Go and NoGo conditions started around 220 ms and continued until about 550 ms post-target onset. Conversely, in session B, condition-specific microstates, expected to reflect in MI the putative processes of the voluntary rehearsal and of the concomitant inhibition of motor programs, were contained in a time window around 230-360 ms post-target onset. Critically, statistical source analyses comparing microstates different among conditions in these time windows, revealed the activation in both NoGo and MI trials of the main foci of motor inhibitory control, namely of pre-SMA and rIFG, but with dissimilar timing and patterns of modulation. These results provide new evidence that basic nodes of an inhibitory network are shared in overt and covert actions, and at the same time underscore a different functional interaction of these areas during the two motor performance modalities.

We will discuss our findings regarding inhibition in MI condition in the light of the functional interpretation of the activities emerged during the overt Go/NoGo task. Indeed, our results could also contribute to clarify processes and related neural substrates activated during time periods overlapping with NoGo-N2 and NoGo-P3, which have been related to motor inhibition of overt actions in Go/NoGo tasks, but which to date are still highly debated.

In Go/NoGo tasks, inhibitory processes are difficult to disentangle from overlapping operations related to executive control: indeed, inhibition in such tasks could be contextualized in terms of a goal-driven response selection, considering the NoGo condition as a form of active voluntary response [8]. Accordingly, our analyses showed that during the overt Go/NoGo task, motor inhibitory control was integrated in the framework of a perceptual decision-making process, and that it was built up in two steps. The first step was an early "decisional" phase, in the 220-300 ms post-target onset (overlapping with NoGo-N2 time range, Figure 2), representing the selection of the NoGo response option and the triggering of

the inhibitory process; the second step was a subsequent “implementational” phase in which the inhibition was enacted and maintained, in the time range of NoGo-P3 (Figure 2).

Statistical source comparison in session A between condition-specific microstates of the early decisional phase showed simultaneous activity in several brain areas, suggesting different concomitant cerebral operations. In particular, comparing NoGo-Map 5 and Go-Map 6 we found stronger activity in NoGo condition in left prefrontal cortex, left dPMC, left pre-SMA and right IPL. These sources likely represent the tight integration between frontoparietal circuits, engaged in visuomotor transformations for the representation of motor response options, and high level prefrontal areas, providing parallel top-down signals biasing the final selection of the correct inhibitory response [120]. In this context, the left DLPFC would retrieve working memory information about task goals and contingencies, providing top-down guidance to response-selection operations ongoing in frontoparietal areas [121]. In particular, the contribution of the DLPFC would be necessary to successful response inhibition in situations with increased cognitive demand [122], as in the cued CPT type of Go/NoGo task used in the present study.

At the same time, the right IPL, through reciprocal interactions with prefrontal cortex and dPMC, would both provide and maintain selected representations of stimulus-response associations and participate in attentional reorienting to behaviourally relevant stimuli [123], focusing cognitive resources at the presentation of the NoGo target. Of note, it has been proposed a role of the right PPC in situations of response conflict between action plans, and in particular in the presence of competition between stimulus-driven action representations and voluntary control of behaviour [124; for review, see 125].

Likely, the higher activity in NoGo with respect to Go condition in left dPMC during the early decisional phase could be inscribed in this perspective. Left dPMC plays a pivotal role in conditional motor behaviour, in which response selection relies on arbitrary visuomotor

associations [23, 126]. This area would encode prelearned stimulus-response associations and provide such predictive information to other reciprocally connected nodes of sensorimotor system, such as the PPC, during the goal-oriented response selection [120]. In this regard, it has been shown that also NoGo stimuli can automatically trigger task-response representations [127], which possibly are usefully integrated during response elaboration, but which also would require active inhibition to avoid overt unwanted movements.

The dPMC could encode both response-specific motor programs and their concomitant inhibition, in an intrinsic bottom-up loop: this putative form of reactive automatic inhibition has been proposed as an "impulse control" mechanism [128], aimed at the inhibition of the selected motor program during preparation of a delayed response. Our data further extend this proposed function, suggesting that a similar automatic mechanism could be involved also during the reactive inhibition of the NoGo response. To date, ample evidence sustains the role of left dPMC in inhibition of overt actions: activation in this area has been previously reported in NoGo condition in EEG [e.g., 46] and fMRI studies [e.g., 129], and also in single-unit neuronal recording in monkeys during a countermanding reaching task [24]. In our study, such putative inhibitory activity of left dPMC was sustained during NoGo condition, from about 220 to 535 ms, possibly with a dual function. In the early decisional phase of inhibitory control, it would have favoured the selection of NoGo response option, providing a direct inhibition of motor response programs automatically triggered at stimulus presentation. Later on, its sustained activity would have contributed to the effective enactment of the selected NoGo decision, during the "implementational" phase of inhibition. Furthermore, left dPMC engagement in MI condition emerged by contrasting MI-Map 5 and Go-Map 6. The enhanced activity in this area in both NoGo and MI with respect to Go condition, points to its role in motor inhibition in both overt and covert actions, but likely with a specific task-dependent degree or pattern of engagement, according to different strength or type of inhibition required

in covert and overt motor modalities. The putative automatic loop of activation-inhibition of motor representations coded by left dPMC, during MI could have contributed to both the voluntary rehearsal and concurrent inhibition of the covert action. Nevertheless, its role would be more relevant in NoGo condition, which requests additional inhibitory resources. Indeed, in session A the risk that stimulus-elicited motor representations could reach the threshold for triggering undesired overt responses was higher as compared to session B, because in the former participants were primed to the possibility to make an overt response, while in the latter just a covert action was involved.

Of note, dPMC is one of the NMAs, i.e., cortical motor regions whose electrical stimulation induces the inability to perform voluntary movements or sustained muscle contraction, without muscular weakness [25; for review, see 130]. Classically, the two main NMAs were identified in correspondence of the IFG ("primary NMA") and of the pre-SMA ("supplementary NMA") [130], which also represent the principal nodes of the hypothesized motor inhibitory network, and whose activity emerged during NoGo and MI conditions in our paradigm. In particular, in the overt Go/NoGo task higher activity in pre-SMA emerged in NoGo-Map 5 with respect to Go-Map 6, during the early phase of inhibition.

Due to its large connection with prefrontal, PPC and other premotor areas [131], the pre-SMA is optimally situated to transform information about the appropriateness of the response options elaborated in parietopremotor circuits and prefrontal regions, into the selection or preparation of the correct response. Accordingly, the pivotal role of the pre-SMA in motor control would be the resolution of the competition between alternative response options, whose neural representations could be activated by external stimuli as well as by internal biases [7, 9]. The pre-SMA would enact an inhibitory mechanism aimed at the suppression of motor representations of unwanted responses, to favour the selection of the most appropriate one [9, 132]. In this view, the motor inhibition of NoGo task would just represent a particular

instantiation of this general pre-SMA activity. Such proposed inhibitory activity of pre-SMA occurs within a network including the rIFG and BG [3], but to date, the temporal hierarchy of activation of these regions is still unclear [10, 133]. In our study, the high temporal resolution of EEG technique allowed us to define the sequential engagement of these areas during our overt Go/NoGo task, namely in the pre-SMA first and in the rIFG subsequently. Indeed, a higher activation in rIFG emerged in NoGo-Map 8 with respect to Go-Map 7. Critically, NoGo-Map 8 was comprised in the 318-432 ms post-target onset: the higher rIFG activity during this microstate could effectively reflect a real-time motor inhibitory mechanism, as it started about 100 ms before the mean Go EMG onset (415 ± 69 ms post-target onset).

A new crucial finding of our study is the activation during MI of the main foci of the hypothesized circuit underpinning inhibition of overt actions (namely, the pre-SMA and rIFG), which emerged by statistical source comparison between MI-Map 5 and NoGoMI-Map 4.

Theoretically, alternative explanations for pre-SMA and rIFG activations in NoGo and in MI conditions could be argued [e.g., 6, 27, 134]: in particular, they could be accounted for by different levels of conflict or of cognitive and attentional load between conditions, due to a higher frequency of Go/MI with respect to NoGo/NoGoMI targets. In fact, our data rule out such alternative hypotheses. Indeed, the influence of the "categorical probability" (related to the class to which stimuli are assigned by task instructions) [34] can be excluded, since Go and NoGo trials in session A and MI and NoGoMI trials in session B had equal frequency. Moreover, also the potential influence of the "single stimulus probability" [34] (i.e., higher level of conflict or cognitive and attentional effort needed to individuate each of the 10 different infrequent "noX" letters used as NoGo and NoGoMI targets, with respect to the more frequent "X" letter, representing Go and MI targets) can be excluded. Indeed, higher activity in pre-SMA and rIFG were found in conditions instructed by targets with different

"single stimulus probability", since the 10 infrequent "noX" letters instructed the NoGo condition and conversely the frequent "X" letter instructed the MI condition.

Our data further extend the previously proposed similarities between the neural substrates of covert and overt actions [74] also in the context of the cerebral mechanisms underpinning their motor inhibition. Nonetheless, at the same time important divergences in the inhibition of overt and covert motor performance emerged, suggesting different patterns of temporal recruitment of inhibitory areas, tuned with the overt or covert motor context and with the intended final task goal.

Indeed, the inhibitory control of the overt action in NoGo condition sequentially developed in early pre-SMA-related decisional phase and late rIFG-related "implementional" phase. On the contrary, during MI, inhibition seemed to be carried out in a single step, with the concomitant engagement of pre-SMA and rIFG, as revealed by statistical comparison of MI-Map 5 vs. NoGoMI-Map 4. Hence, the inhibition of the rehearsed motor programs during MI appeared strictly intertwined with response-selection operations. This sort of prewired coupling between these two processes suggests that an inhibitory mechanism related to the rIFG might have been integrated *a priori* into the process of selection and voluntary rehearsal of movement representations, as an intrinsic component of the MI enactment. Of note, MI could be viewed as a particular type of covert action in which the movement representation is voluntarily rehearsed and concurrently automatically inhibited. Inhibition during MI could be considered "automatic" since it runs to completion autonomously, without volitional effort [135]. Nevertheless, although when individuals imagine they do not deliberately think to put into effect inhibitory commands *per se*, they are aware that they will not overtly move. Hence, motor inhibition during MI could yet be included in a goal-oriented "covert modality" of motor performance. This would represent a form of "contingent" or "conditional" automaticity [135, 136], wherein a cerebral process, even if triggered and implemented

automatically, is still conditioned on contingently activated top-down goals. In line with this hypothesis, previous studies [137-139] demonstrated that cerebral foci for the controlled inhibition of overt actions, such as the pre-SMA and rIFG, can be triggered unconsciously but yet with a "contingent" automaticity, depending on the presence of a specific activated executive set [139]. Indeed, it has been shown that rIFG activity can be automatically triggered by stimuli that were previously associated with stopping, without the requirement of actual top-down controlled motor inhibition [137]. Moreover, also an unconscious, strongly masked NoGo stimulus can activate the pre-SMA and IFG [138].

Possibly, in our study during session B, the instructed covert performance modality itself could have intrinsically predisposed the rIFG activation in response to the MI target, allowing an automatic but still goal-oriented inhibition to be implemented during the voluntary rehearsal of motor representations. This view is in accord with the results of a previous EEG study [103] that revealed the influence on information processing of the anticipated overt and covert motor modalities, not only at a late stage of motor performance enactment, but already at an early stage of stimulus processing. Our data further extend these findings to a motor inhibitory perspective: the performance modality of the possible incoming movement, contained in the instructed task goals, likely *ab initio* differentially predisposed an intrinsic reorganization of the parietofrontal areas designated for sensorimotor transformations and for motor inhibitory control in the two sessions.

Of note, these conclusions go in the direction of a "proactive" control account. In the proactive modality, inhibitory circuits could be primed by predictive cues in preparation for the upcoming inhibition [3, 16] without being effectively implemented. This would create a "proactive inhibitory set" [3, 16] through different cortical-BG circuits, allowing inhibition to be more quickly reactively triggered at the presentation of inhibitory signals. Accordingly, it has been shown that proactive and reactive inhibition engage partially overlapping cerebral

networks, including the pre-SMA, rIFG, IPL and the BG [14-16, 18]. Nonetheless, exact mechanisms and functional meaning of proactive inhibition have yet to be clarified [e.g., for different hypotheses, see 3, 140]. In our CPT, the "O" cue could have primed the motor inhibitory circuit or its parts, favouring the reactive triggering of the inhibitory control when required, namely, at NoGo target onset for the controlled inhibition of overt actions, and at MI target onset, for automatic inhibition of ongoing motor representations. With regard to the latter condition, the concomitant activation of the pre-SMA and rIFG suggests a primed insertion, into the preselected covert modality of motor performance, of an inhibitory mechanism (likely underpinned by the rIFG), which could be subsequently effectively implemented during MI enactment, in a contingent automatic manner.

To confirm this hypothesis, the analysis of the Experimental Study Part 2 focused on the preparatory phase of our overt and covert Go/NoGo tasks.

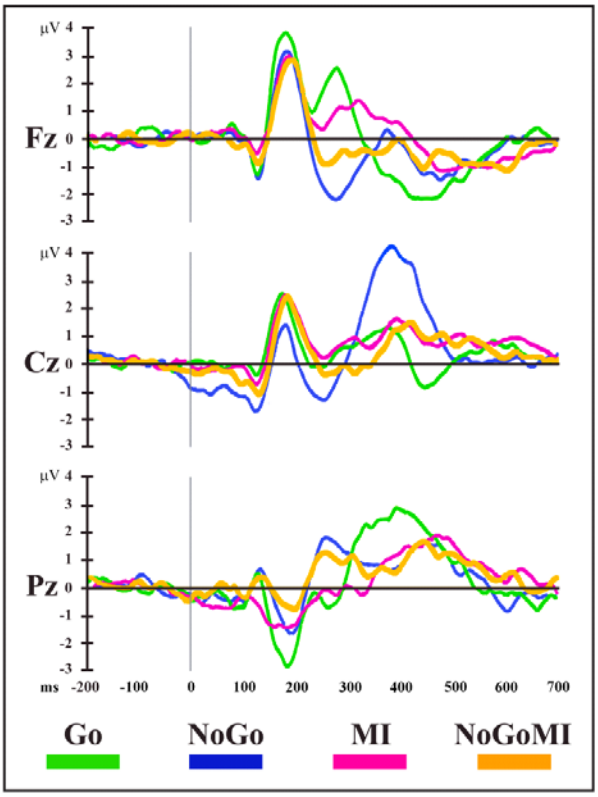

Figure 2. Event related potential (ERP) waveforms. Group-averaged (n = 15) stimulus-locked ERP waveforms (plotted as voltage in μV in function of time in ms, stimulus onset: 0 ms) for the four experimental conditions from Fz, Cz and Pz electrodes. MI: Motor Imagery; NoGoMI: NoGo Motor Imagery.

[Reprinted from: *Angelini M, Calbi M, Ferrari A, Sbriscia-Fioretti B, Franca M, Gallese V, Umiltà MA. Motor inhibition during overt and covert actions: an electrical neuroimaging study. PLoS One. 2015; 10:e0126800*.]

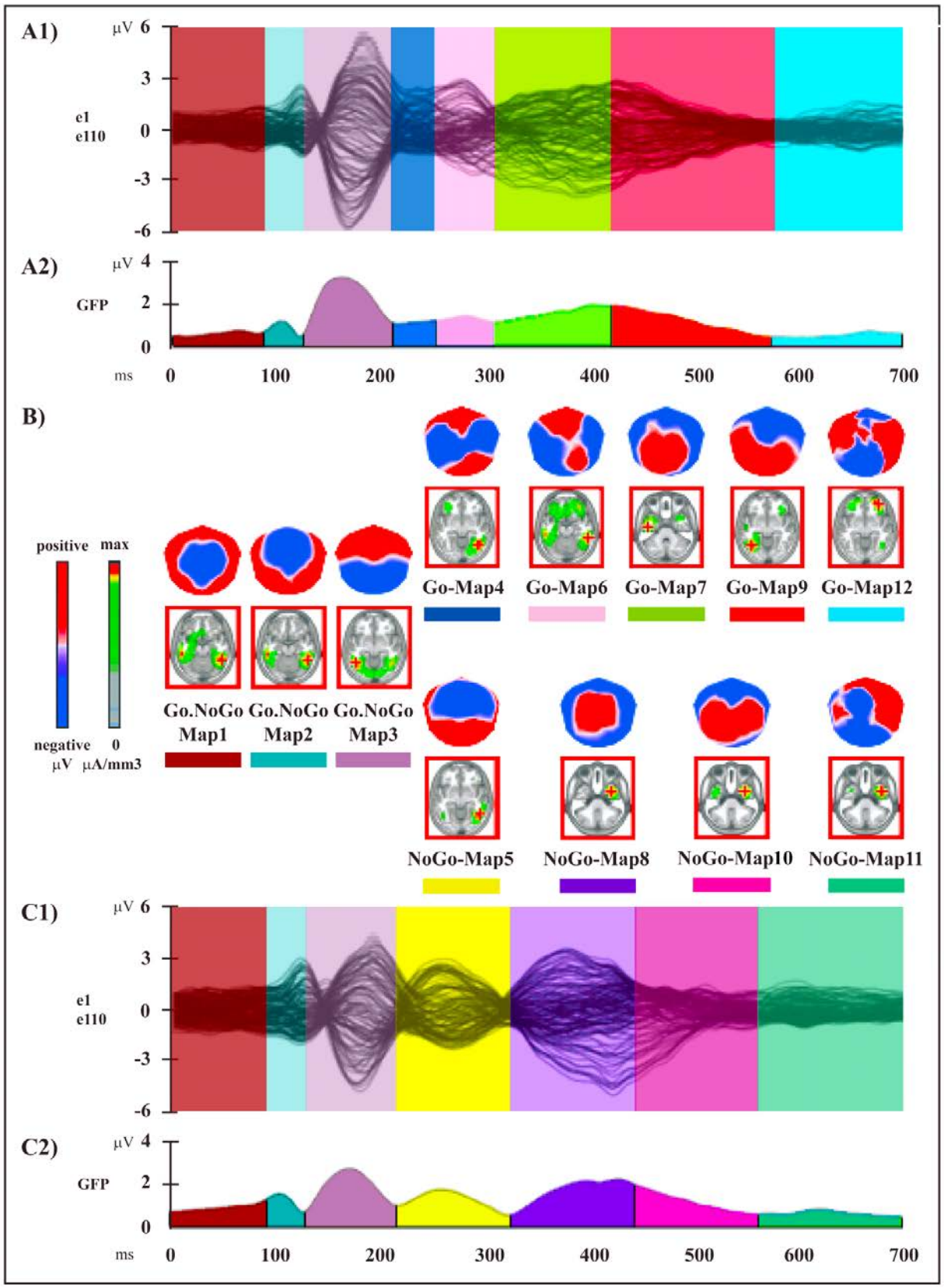
A1)
µV 6
3
0
-3
-6
e1
e110
A2)
µV 4
2
0
GFP
ms 0 100 200 300 400 500 600 700
B)
positive max
negative 0
µV µA/mm3
Go.NoGo Map1
Go.NoGo Map2
Go.NoGo Map3
Go-Map4
Go-Map6
Go-Map7
Go-Map9
Go-Map12
NoGo-Map5
NoGo-Map8
NoGo-Map10
NoGo-Map11
C1)
µV 6
3
0
-3
-6
e1
e110
C2)
µV 4
2
0
GFP
ms 0 100 200 300 400 500 600 700

Figure 3. Electrophysiological results over the 700 ms post-stimulus period (stimulus onset: 0 ms) of session A.

A1, C1. Group-averaged (n = 15) ERP waveforms for Go (A1) and NoGo (C1) conditions, superimposed across the 110 recording channels (e1-e110).

A2, C2. Microstate segmentation results for Go (A2) and NoGo (C2) conditions. The temporal distribution of the microstates in each condition revealed by the spatiotemporal segmentation analysis applied on session A dataset is reported on the curve of the global field power (GFP) (i.e., the variance of the 110 channels over the whole scalp at a given time point). Each microstate and its temporal window are indicated by different colours; the same colour indicates the same microstate.

B. Mean topographic maps and the related mean LAURA source estimations (in red panels) corresponding to each microstate for the group-averaged ERP data.

All topographic maps are plotted with nasion upward and left scalp leftward; each map is scaled separately with respect to its maximum and minimum values to optimise the contrast. The current density maxima resulting from source estimations (green: low current density; red: high current density) are rendered on horizontal slices of MNI152 template brain (left hemisphere on the left side); source estimation for each microstate is independently scaled with respect to its maximum value.

[Reprinted from: *Angelini M, Calbi M, Ferrari A, Sbriscia-Fioretti B, Franca M, Gallese V, Umiltà MA. Motor inhibition during overt and covert actions: an electrical neuroimaging study. PLoS One. 2015; 10:e0126800.*]

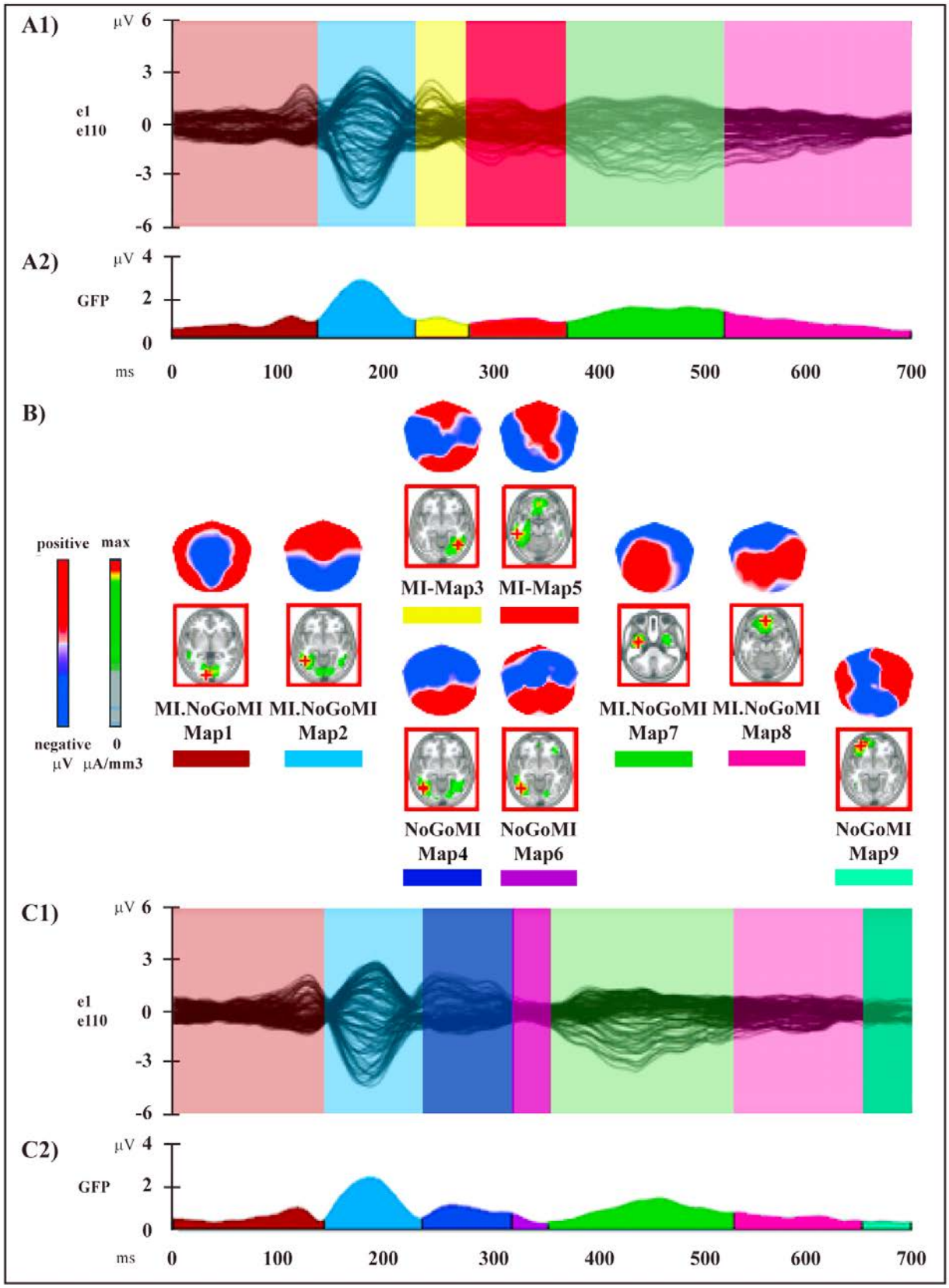
A1)
µV 6
3
0
-3
-6
e1
e110
A2)
µV 4
2
0
GFP
ms
0
100
200
300
400
500
600
700
B)
positive
max
negative
µV
0
µA/mm3
MI.NoGoMI
Map1
MI.NoGoMI
Map2
MI-Map3
MI-Map5
MI.NoGoMI
Map7
MI.NoGoMI
Map8
NoGoMI
Map4
NoGoMI
Map6
NoGoMI
Map9
C1)
µV 6
3
0
-3
-6
e1
e110
C2)
µV 4
2
0
GFP
ms
0
100
200
300
400
500
600
700

Figure 4. Electrophysiological results over the 700 ms post-stimulus period (stimulus onset: 0 ms) of session B.

A1, C1. Group-averaged (n = 15) ERP waveforms for Motor Imagery (MI) (A1) and NoGo Motor Imagery (NoGoMI) (C1) conditions, superimposed across the 110 recording channels (e1-e110).

A2, C2. Microstate segmentation results for MI (A2) and NoGoMI (C2) conditions.

B. The mean topographic maps and the related mean LAURA source estimations (in red panels) corresponding to each microstate for group-averaged ERP data. All other conventions as in Figure 3.

[Reprinted from: *Angelini M, Calbi M, Ferrari A, Sbriscia-Fioretti B, Franca M, Gallese V, Umiltà MA. Motor inhibition during overt and covert actions: an electrical neuroimaging study. PLoS One. 2015; 10:e0126800.*]

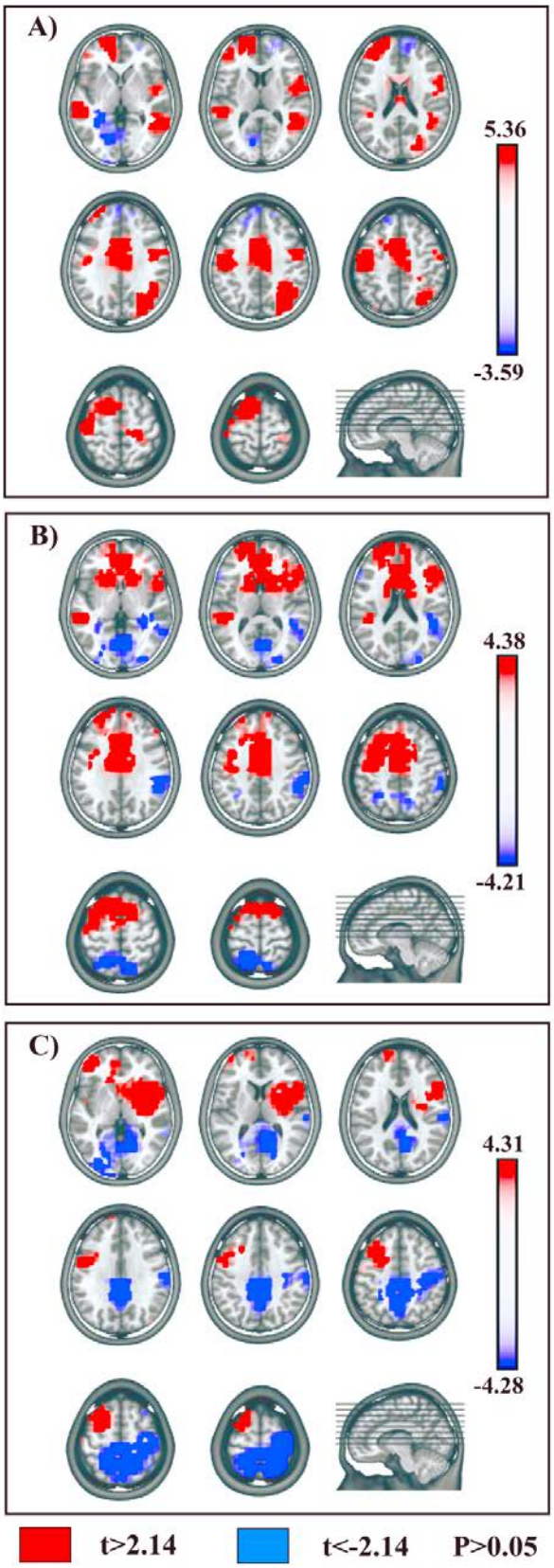
A)
5.36
-3.59
B)
4.38
-4.21
C)
4.31
-4.28
t>2.14
t<-2.14
P>0.05

Figure 5. S**tatistical comparisons of LAURA source estimations between condition-specific microstates (voxel-wise parametric mapping analysis of the inverse solutions): NoGo vs. Go conditions.** All significant voxels are coloured ($t_{(14)} > 2.14$ / < -2.14, $p < .05$): positive *t* values (red colour) indicate higher current source densities in NoGo than in Go condition; negative *t* values (blue colour) indicate higher current source densities in the Go than in the NoGo condition. LAURA solutions are rendered on MNI152 template brain.

A. NoGo-Map 5 vs. Go-Map 6.

B. NoGo-Map 8 vs. Go-Map 7.

C. NoGo-Map 10 vs. Go-Map 9.

[Reprinted from: *Angelini M, Calbi M, Ferrari A, Sbriscia-Fioretti B, Franca M, Gallese V, Umiltà MA. Motor inhibition during overt and covert actions: an electrical neuroimaging study. PLoS One. 2015; 10:e0126800.*]

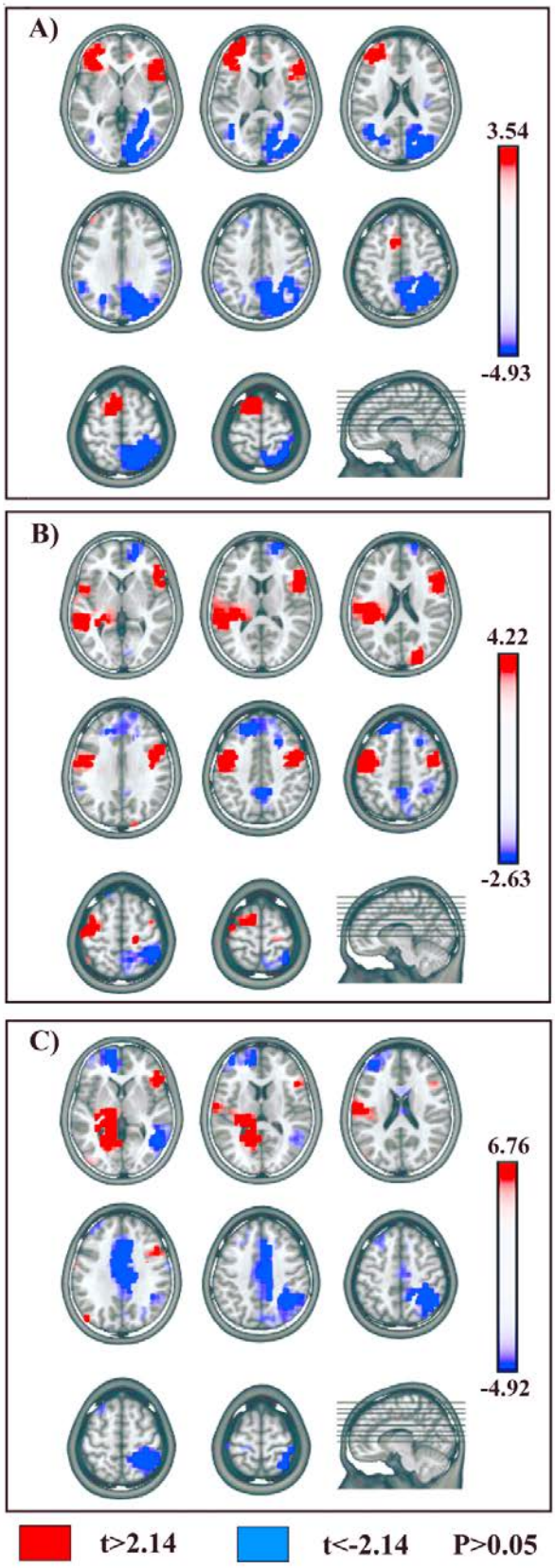
A)
3.54
-4.93
B)
4.22
-2.63
C)
6.76
-4.92
t>2.14
t<-2.14
P>0.05

Figure 6. S**tatistical comparisons of LAURA source estimations between condition-specific microstates (voxel-wise parametric mapping analysis of the inverse solutions)**: **Motor Imagery (MI) vs. NoGo Motor Imagery (NoGoMI), Go and NoGo conditions**. Positive *t* values (red colour) indicate higher current source densities in MI than in the compared condition; negative *t* values (blue colour) indicate higher current source densities in the compared condition than in MI condition. All other conventions as in Figure 5.

A. MI-Map 5 vs. NoGoMI-Map 4.

B. MI-Map 5 vs. Go-Map 6.

C. MI-Map 5 vs. NoGo-Map 5.

[Reprinted from: *Angelini M, Calbi M, Ferrari A, Sbriscia-Fioretti B, Franca M, Gallese V, Umiltà MA. Motor inhibition during overt and covert actions: an electrical neuroimaging study. PLoS One. 2015; 10:e0126800.*]

Microstate	Talairach and Tournoux coordinates (x,y,z mm)	Brain region label
Go.NoGo Map1	48, -48, -13	Right fusiform gyrus, BA 37
Go.NoGo Map 2	48, -48, -13	Right fusiform gyrus, BA 37
Go.NoGo Map 3	-48, -55, -6	Left middle occipital gyrus, BA 19
Go-Map 4	41, -62, -6	Right fusiform gyrus, BA 37
NoGo-Map 5	48, -55, -6	Right middle occipital gyrus, BA 19
Go-Map 6	56, -41, -13	Right middle temporal gyrus, BA 20
Go-Map 7	-48, -12, -27	Left inferior temporal gyrus, BA 20
NoGo-Map 8	33, 1, -35	Right inferior temporal gyrus, BA 20
Go-Map 9	-41, -62 ,-6	Left fusiform gyrus, BA 37
NoGo-Map 10	33, 1, -35	Right inferior temporal gyrus, BA 20
NoGo-Map 11	41, 1, -35	Right middle temporal gyrus, BA 38
Go-Map 12	33, 47, -11	Right middle frontal gyrus, BA 11

BA: Brodmann Area

Table 1. Talairach and Tournoux coordinates and corresponding brain region label of current source density maximum of each mean template map resulting from segmentation analysis applied to Go and NoGo dataset (session A).

Microstate	Talairach and Tournoux coordinates (x,y,z mm)	Brain region label
MI.NoGoMI-Map 1	-11, -91, 1	Left lingual gyrus, BA 17
MI.NoGoMI-Map 2	-48, -55, -6	Left middle occipital gyrus, BA 19
MI-Map 3	41, -62, -6	Right fusiform gyrus, BA 37
NoGoMI-Map 4	-48, -62, -6	Left middle occipital gyrus, BA 37
MI-Map 5	-56, -33, -14	Left inferior temporal gyrus, BA 20
NoGoMI-Map 6	-48, -62, -6	Left middle occipital gyrus, BA 37
MI.NoGoMI-Map 7	-41, -5, -34	Left middle temporal gyrus, BA 21
MI.NoGoMI-Map 8	-3, 46, -18	Left medial frontal gyrus, BA 11
NoGoMI-Map 9	-33, 47, -11	Left middle frontal gyrus, BA 11

BA: Brodmann Area

Table 2. Talairach and Tournoux coordinates and corresponding brain region label of current source density maximum of each mean template map resulting from segmentation analysis applied to Motor Imagery (MI) and NoGo Motor Imagery (NoGoMI) dataset (session B).

Chapter 4

Experimental Study Part 2

Analysis of the preparatory phase

4.1 EEG analysis methods

In the "Experimental Study Part 2" (analysis of the preparatory phase), we applied nonparametric randomization statistic on two parameters describing the scalp global electric field: a) the GFP (Global Field Power), for the assessment of modulations in electric field strength; b) the DISS (Global Map Dissimilarity), for the assessment of modulations in electric field topography (see also "2.1 Aims of the study"). Statistical analysis applied on these global topographic measures allows one to distinguish whether simple modulation in response strength or, conversely, dissimilar scalp electric field topographies underpin different elicited EEG activities between experimental conditions. Hence, this approach provides a more objective definition of time windows for source analysis, relying on the statistical proof that the electric fields are different and thus produced by different neural generators [105].

The GFP is the root mean square across the average-referenced electrode values at a given instant in time. In other words, GFP is the standard deviation of the potentials at all electrodes of an average-referenced map, and mathematically it is defined as [111]:

$$GFP = \sqrt{\frac{\sum_{i}^{N} = 1 \quad (u_i - \overline{u})^2}{N}}$$

ui: voltage of the map *u* at the electrode *i*

$\bar{u}$: average voltage of all electrodes of the map *u*

N: number of electrodes of the map *u*.

In the case of ERPs, the resultant GFP waveform is a measure of potential (μV) as a function of time. Scalp potential fields with prominent peaks and troughs and steep gradients will result in high GFP, while maps with a "flat" appearance and low gradients have low GFP. GFP is a measure of the map at each moment in time: displaying GFP over time allows identifying periods of high signal-to-noise ratio, corresponding to high global neuronal synchronization.

The GFP represents a single, reference-independent measure of the global strength of the recorded potential across the electrode montage [105]**.** On the contrary**,** it is uninformative about the distribution of the potential across the electrode montage, namely where large and small potentials are measured. Therefore, on the one hand a GFP modulation does not exclude the possibility of a contemporaneous change in the electric field topography. On the other hand, equivalent GFP values do not exclude the possibility of concomitant topographic modulations. The observation of a GFP modulation without a concomitant topographic modulation can be interpreted as a difference of the number of synchronously activated but statistically indistinguishable generators across experimental conditions [105].

Conversely, the DISS is a measure of configuration differences between two electric fields, independently of their strength. The DISS is the square root of the mean of the squared differences between the potentials measured at each electrode (versus the average reference),

each of which is first scaled to unitary strength by dividing by the instantaneous GFP, since only topographic differences are taken into account.

Mathematically, it is defined as [111]:

$$DISS = \sqrt{\frac{1}{N}\sum_{i=1}^{N}\left\{\frac{u_i - \bar{u}}{\sqrt{\sum_{i=1}^{N}(u_i - \bar{u})^2/N}} - \frac{v_i - \bar{v}}{\sqrt{\sum_{i=1}^{N}(v_i - \bar{v})^2/N}}\right\}^2}$$

ui: voltage of map u at the electrode i

vi: voltage of map v at the electrode i

$\bar{u}$: average voltage of all electrodes of map u

$\bar{v}$: average voltage of all electrodes of map v

N: total number of electrodes.

DISS values can range from 0 to 2, where 0 indicates topographic homogeneity when two maps are equal and 2 indicates topographic inversion when two maps have the same topography with reversed polarity**.**

The presence of topographic differences between two maps independently of their strength indicates that the two maps are generated by a different configuration of cerebral sources. Displaying the DISS over time allows defining periods of map stability and of map changes. Indeed, DISS tends to be inversely correlated with the GFP, since DISS is high when GFP is

low. Maps show a stable topography during high GFP and change the configuration when GFP is low (i.e., during concurrent DISS peaks).

The GFP and DISS measures can be used to statistically evaluate differences in strength and topography over time or between experimental conditions or population groups, in a completely reference-independent way and without the *a priori* selection of time periods, electrodes or components of interest for analyses. Of note, in order to assess differences in GFP at each time point, both parametric and nonparametric statistic tests can be used. Conversely, for the statistic assessment of topographic differences using the DISS as the dependent measure, a nonparametric statistical test is required. Indeed, **t**he DISS is a measure of the distance between two vectors (each of which represents one electric field topography), rather than a separate measure for each compared condition, hence mean and standard error of topography for each condition cannot be calculated [105, 111]. The nonparametric analysis of the DISS between two maps is called "topographic ANOVA" (TANOVA), although it does not involve an analysis of the variance, but a randomization test [105, 111]. Randomization provides a robust nonparametric method to test for differences in any variable without any assumptions regarding data distribution, by comparing the observed dataset with random shuffling of the same values over sufficiently large number of iterations (i.e., permutations). These randomized data are one instance of a set of observations that one could have made under the null hypothesis, and the effect size obtained from randomized data is one instance of an effect size obtained under the null hypothesis. By repeating the randomization of the data and the computation of the effect size in the randomized data several times, the empirical distribution of the effect size under the null hypothesis is obtained. By comparing the effect size obtained in the real observed data to the empirical distribution of the effect size under the null hypothesis, this method allows determining the probability that the data might be observed by chance. This probability is defined as the number of random effect sizes that are

larger than or equal to the observed effect size, divided by the total number of randomizations. If the probability is high, the null hypothesis is accepted and the alternative hypothesis is rejected, since it lacks statistical evidence [141]. Therefore, being a randomization-based method, the procedure for the TANOVA involves different steps. The first step is the calculation of an empirical distribution of the DISS values under the null hypothesis. To do that, the maps of the single subject are first randomly reassigned to different experimental conditions (permutations of the data). Then, the group-averaged ERPs are recalculated and finally, the resulting DISS values for these randomized group-averaged ERPs are measured. In order to obtain reliable results with randomization, at least 1000 permutations are required if the critical threshold of the *p* value is 0.05 and 5000 randomizations if the critical *p* value is 0.01 [142]. In a within-subject design, the permutation of the maps is done within the subjects, while the permutation is done across subjects in group comparisons. Then, the DISS value from the real group-averaged ERPs is compared with the values from the empirical distribution to determine the likelihood that the empirical distribution has a value higher than the DISS from the real group-averaged ERPs. This procedure is repeated for each time point. By statistically proving that the scalp topographies are different, the TANOVA provides a reliable means of determining whether and when the brain networks activated by different experimental conditions differ, because electric field changes are indicative of changes in the underlying generators**.**

Given this theoretical background, the present study is based upon a global scalp electric field statistical analysis, which has two principal advantages: 1) it is completely reference independent; 2) it allows the statistical assessment of the likely neurophysiological mechanisms (i.e., topographic and/or strength modulation) underpinning the observed effects [105]. In addition, for completeness and as a preliminary step in determining the time course of ERP response modulations, a global ERP waveform analysis was performed, to minimize

the possibility of missed effects related to the preselection of specific electrodes and time periods used in canonical ERP waveform analysis.

All the statistical analyses were conducted using Cartool software [111].

4.1.1 Global ERP amplitude analysis

The global amplitude analysis of the ERP waveforms was conducted by means of point-wise paired *t* tests computed on amplitudes of the single-subject ERP averages of the two sessions, at each electrode and time point. The statistical significance level was set at $p < .05$ and a 10 contiguous data points temporal criterion (20 ms at our 500 Hz sampling rate) for the persistence of significant effects was applied [143]. Only differences over at least five contiguous electrodes within nine clusters (shown in the inset in Figure 7) reaching the statistical significance level were retained.

4.1.2 Global scalp electric field analysis

Two statistical analyses were conducted on the global electric field:

a) assessment of modulations in electric field strength, as measured by the instantaneous GFP. Point-wise paired randomizations were conducted on the GFP of single-subjects ERP averages between sessions at each time frame, with a significance level set at $p < .05$ and a temporal acceptance criterion of 20 ms of consecutive significant difference.

b) assessment of modulations in electric field topography, measuring DISS. Point-wise paired randomizations (TANOVA) were performed on the DISS values between sessions, calculated for each time point and each participant data, with a significance level set at $p < .05$ and a temporal acceptance criterion of 20 ms of consecutive significant difference.

In both analyses, the point-wise randomization tests ran 1000 permutations per data point for the significance level of $p < .05$ [142].

These two analyses allowed a neurophysiological interpretation of the ERP modulations: indeed, differences in GFP without simultaneous topographic changes are indicative of amplitude modulation of statistically indistinguishable generators between experimental conditions. Conversely, topographic differences between conditions, with or without concomitant GFP modulations, necessarily derive from changes in the configuration of the underlying active brain sources [105].

4.1.3 Source Analysis

The results of the TANOVA defined time periods during which intracranial sources were estimated, using a distributed linear inverse solution based on a LAURA regularization approach [117]. The solution space was calculated on a locally spherical head model with anatomical constraints (L-SMAC) [118] and comprised 3001 solution points (voxels) homogeneously distributed within the brain structures of the Montreal Neurological Institute (MNI152) average brain. All solution points were labeled with their Talairach and Tournoux coordinates [119] as well as their anatomical labels.

Intracranial source estimations for each participant and session over time windows defined by the TANOVA were then statistically compared by means of a "voxel-wise parametric mapping analysis" [114]. To do that, individual ERP data were averaged over time periods of significant topographic modulation, in order to generate a single data point per period for each participant and session. The LAURA current density source estimations for each solution point were then contrasted by means of paired *t* tests. Solution points with *p* values < .05 ($t(14) > 2.14 / < -2.14$) were considered significant; in addition, a cluster threshold of at least 10

contiguous activated solution points was applied. Source analyses were performed using Cartool software [111].

4.2 Results

The electrophysiological results of global amplitude and scalp electric field analyses and the results of source analyses are reported separately. Significant results of the statistical comparisons of LAURA source estimations (voxel-wise parametric mapping analysis) in significant TANOVA time periods are reported, with *t* and *p* values, Talairach and Tournoux coordinates (x,y,z) [119] and anatomical labels of solution points with the local maximum different activities.

4.2.1 Electrophysiological Results

The group-averaged ERPs for session A and session B are shown in Figure 7A, superimposed across the 110 recording channels (e1-e110).

The global amplitude analysis (Figure 7B) revealed three periods of significant ERP modulation:

1) from 188 to 222 ms after cue onset, over anterior clusters of electrodes, at a right and midline location, and over posterior clusters of electrodes, at a left and midline location;

2) from 246 to 324 ms after cue onset, at all scalp regions;

3) from 346-558 ms after cue onset, in particular over posterior clusters of electrodes from 352 to 458 ms, and over frontal and central clusters of electrodes during the whole time window.

The analysis of the GFP (Figure 7C, upper plot) showed three periods of sustained difference between sessions, reflecting a strength modulation with a stronger activity in session A:

1) from 95 to 158 ms;

2) from 350 to 622 ms;

3) from 632 to 674 ms after cue onset.

The TANOVA (Figure 7C, lower plot) revealed three phases of significant topographic differences between sessions, reflecting the activation of distinct configurations of intracranial generators:

1) from 192 to 220 ms;

2) from 258 to 306 ms;

3) from 438 to 472 ms after cue onset.

Mean topographic maps of the group-averaged ERP data of session A and B, corresponding to each significant TANOVA time interval, are shown in Figure 7D.

In summary (Figure 7), GFP and DISS analyses revealed that different cerebral generators underpinned the first (between about 190-220 ms after cue onset) and the second (between about 245-325 ms) periods of amplitude modulation between sessions, which overlapped with periods of significant different scalp field topography. The third prolonged amplitude modulation (between 345-560 ms after cue onset) was characterized by both strength and topographic differences between sessions.

4.2.2 Source Analysis

For the first time period of different topography (192-220 ms after cue onset), significant higher activity in session A as compared with session B (Figure 8A, red) was found in four cerebral clusters:

1) left precentral and postcentral gyri, extending toward middle frontal gyrus (BAs 3, 4, 6) ($t_{(14)} = 3.72$; $p = .002$; x,y,z: -33,-16,46; left precentral gyrus, BA 4);

2) left occipital extrastriate cortex, encompassing cuneus and middle occipital gyrus (BA 18) ($t_{(14)}$ = 3.71, p = .002; x,y,z: -18,-90,31; left occipital cuneus, BA 18);

3) left superior temporal gyrus (BA 22) ($t_{(14)}$ = 3.37, p = .005; x,y,z: -48,-39,12; left superior temporal gyrus, BA 22);

4) left prefrontal cortex, encompassing DLPFC and frontopolar cortex (BAs 9, 10) ($t_{(14)}$ = 2.88, p = .012; x,y,z: -18,27,29; left medial frontal gyrus, BA 9).

In the second significant TANOVA period (258-306 ms after cue onset), higher activity in session A (Figure 8B, red) was found in three clusters:

1) bilateral PPC, encompassing the SPL and precuneus (BA 7) ($t_{(14)}$ = 4.38, p = .0006; x,y,z: 26,-53,40; right SPL, BA 7);

2) bilateral dACC ($t_{(14)}$ = 2.83, p = .013; x,y,z: -11,19,23; anterior cingulate cortex, BA 24)

3) right DLPFC, encompassing superior and medial frontal gyri (BA 9) ($t_{(14)}$ = 2.76, p = .015; x,y,z: 11,41,29; right medial frontal gyrus, BA 9).

Higher activity in session B (Figure 8B, blue) was found in two clusters:

1) right anterior temporal and temporopolar cortex, encompassing superior, middle and inferior temporal gyri (BAs 20, 21, 38) ($t_{(14)}$ = -3.89, p = .002; x,y,z: 48,1,-35; right middle temporal gyrus, BA 21);

2) right orbitofrontal cortex, encompassing rectal and middle frontal gyri (BA 11) ($t_{(14)}$ = -3.56, p = .003; x,y,z: 11,39,-24; right rectal gyrus, BA 11).

In the third period of topographic modulation (438-472 ms after cue onset), significant higher activation in session A (Figure 8C, red) was found in two cerebral clusters:

1) left pre-SMA (BA 6) ($t_{(14)}$ = 2.88, p = .012; x,y,z: -3,21,58; left superior frontal gyrus, BA 6);

2) left VLPFC (BAs 45, 47) ($t_{(14)}$ = 2.68, p = .018; x,y,z: -56,25,2; left IFG, BA 45).

Higher activity in session B (Figure 8C, blue) was found in two cerebral clusters:

1) rIFG (BA 45) ($t_{(14)}$ = -2.77, p = .015; x,y,z: 56,18,9; rIFG, BA 45);

2) left fusiform gyrus (BA 37) ($t_{(14)}$ = -2.33, p = .035 ; x,y,z: -33,-48,-13; left fusiform gyrus, BA 37).

4.3 Discussion

The aim of the "Experimental Study Part 2" was to evaluate whether different response strategies were triggered in the preparatory phase of two different cued Go/NoGo tasks, requiring the execution or inhibition of an overt motor response (AE) in session A and of a covert motor response (MI) in session B, respectively. In particular, we aimed at clarifying whether the preparatory cues proactively elicited putatively similar inhibitory circuits that appeared to be subsequently involved in the withholding of the overt response in NoGo trials and in the inhibition of overt movement execution during the MI trials (see "3.3 Discussion" in Experimental Study Part 1).

Our results confirmed in both sessions the priming of cerebral regions pertaining to such putative inhibitory network that were reactively triggered in the following response phase; nonetheless, difference in the preparatory strategies between the two sessions emerged, depending on the intended "overt" or "covert" performance modality of the possible incoming motor response.

The TANOVA showed that topographic differences in preparatory activities between the two sessions started around 190-220 ms after the cue onset. In this time period, the higher activation in session A of a motor region encompassing the left motor and premotor cortex (Figure 8A), revealed by source analysis, could index the cue-elicited priming of the incoming overt Go-response representations. This result is consistent with evidence that motor programs can be automatically triggered by visual warning signals [144, 145],

preparing the motor system for the execution of the selected response at subsequent target onset. Nevertheless, to prevent wrong cue-triggered overt movements during the foreperiod, a concomitant inhibitory mechanism is required. In this regard, it has been hypothesized that the premotor cortex could encode both response-specific motor programs and their concomitant automatic inhibition [128]. The activation of the left dPMC that emerged in our results is consistent with this proposed "impulse control" mechanism [128], triggered during the preparation of a delayed response and aimed at maintaining in check the selected motor program until the onset of the imperative signals. This mechanism would represent: "*. . .a self-contained process (. . .) where the activation of a response representation automatically triggers a corresponding inhibitory tag*" [128].

It is worth noting that in the present paradigm the cue did not specify the identity of incoming targets, acting as a generic warning signal and introducing a conflict between representations of the possible forthcoming responses. Indeed, in the second TANOVA time period, higher activity in session A emerged in cerebral areas that have been related to conflict processing, namely the right PPC and the dACC (Figure 8B). It has been proposed that the right PPC might be relevant in situations of conflict between action plans, and in particular in the presence of competition between stimulus-driven action representations and the voluntary control of behaviour [124; for review, see 125]. Moreover, in agreement with the "conflict monitoring hypothesis" [36, 146], the dACC would provide an online signal between contrasting cue-elicited Go and NoGo task-goal representations, recruiting cerebral areas for the resolution of such conflict and the selection of appropriate response, such as the pre-SMA. A similar pattern of activations, including the left DLPFC, the left dPMC and the right parietal lobe also emerged during the NoGo condition in the subsequent response phase. These sources likely represent the functional interplay between prefrontal and frontoparietal regions engaged in visuomotor transformations and in the representation of competing Go and

NoGo response options. These regions could send information to other areas engaged for the resolution of such conflict, like the pre-SMA. This whole mechanism, preactivated by the cue in the preparatory phase, could be reactively triggered at the presentation of the NoGo signals, facilitating the perceptual decision making and the selection of the correct response, i.e., the overcoming of the prepared Go motor response.

In this regard, it has been hypothesized that the pivotal function of the pre-SMA in motor preparation and control is the resolution of conflict within a contingent set of competitive response plans [7, 9], and that its putative role in response inhibition could represent a particular instantiation of this general function [8]. Accordingly, a higher activation of the pre-SMA emerged in session A in the following third TANOVA time interval (Figure 8C). Although these data point to the involvement of the pre-SMA in proactive inhibition of overt actions, the exact role of this area remains unclear. The pre-SMA could set up the nodes of the inhibitory network in advance, favoring their speeded activation when inhibition is needed [15]. The pre-SMA could also participate in the modulation of the threshold of Go response and of the level of excitability of the motor system [147, 148], in the presence of conflicting instructions, or when inhibition is a possible response option. Regardless of the specific mechanism involved, the pre-SMA seems to exert inhibitory control within a network including the rIFG and the BG [3, 133]. Although the rIFG has been claimed as the crucial area for the actual implementation of motor inhibition [3, 133], to date its role in proactive control is still debated. Our analyses did not reveal the activation of the rIFG in the preparation of the overt Go/NoGo task in session A, but just during the subsequent NoGo response (see “3.3 Discussion” in Experimental Study Part 1, pp. 50-51). Taken together, our results sustain the involvement of the rIFG in reactive inhibitory control of overt actions, in agreement with previous studies that did not find the pre-engagement of the rIFG but its activation just during the implementation of inhibition [14, 16, 17]. Hence, the recruitment of

the inhibitory circuit during the preparation of the overt Go/NoGo task was only partial, and limited to the decisional function underpinned by pre-SMA.

On the contrary, the engagement of the rIFG emerged during the preparation of the covert Go/NoGo task, in the third TANOVA interval (Figure 8C). In session B participants knew that their incoming performance would have been limited to covert movements: since they were not requested to overtly move during the whole session B, theoretically there was neither need to activate an inhibitory mechanism in response to the cue, nor to postulate a cue-triggered anticipation of the NoGoMI signal. According to our hypothesis, this finding likely represents the cue-elicited strategy of inhibition of motor outputs in anticipation of the possible incoming imagined covert response. The priming of the rIFG would allow the subsequent automatic enactment of an inhibitory mechanism during MI (see "3.3 Discussion" in Experimental Study Part 1, pp. 51-53), assuring the covert nature of the imagined motor response. Hence, the preparatory strategy for the covert Go/NoGo task was focused on a prioritized recruitment of inhibition of motor outputs in anticipation of the possible incoming imagined response, tuned to the task-related motor goal requiring just a covert action. Conversely, and differently from the overt Go/NoGo task, during session B the early cue-triggered preactivation of the motor or premotor cortex did not emerge. A possible explanation could be related to the fact that in the present paradigm the cue did not specify the identity of subsequent targets: the uncertainty created by such generic cue, about whether or not the MI would have been requested by the incoming target, could have abolished the functional advantage of priming the motor representations for the covert response. In the light of these considerations, future studies comparing overt and covert Go/NoGo tasks using a completely informative cue (i.e., a cue that is associated with a single target and response option) could confirm and further extend our results concerning proactive inhibitory and motor strategies for overt and covert actions. Moreover, a completely informative cue would

minimize superimposed cognitive processes linked to cue analyses, conflict monitoring and resolution and to rules maintenance in working memory.

Finally, due to the low spatial accuracy of EEG technique, further neuroimaging studies with higher spatial resolution should better clarify the involvement of different sectors of complex regions as the PPC and the IFG, and the contribution of subcortical structures such as the BG, the STN or the cerebellum, in the preparation of inhibitory processing in overt and covert actions.

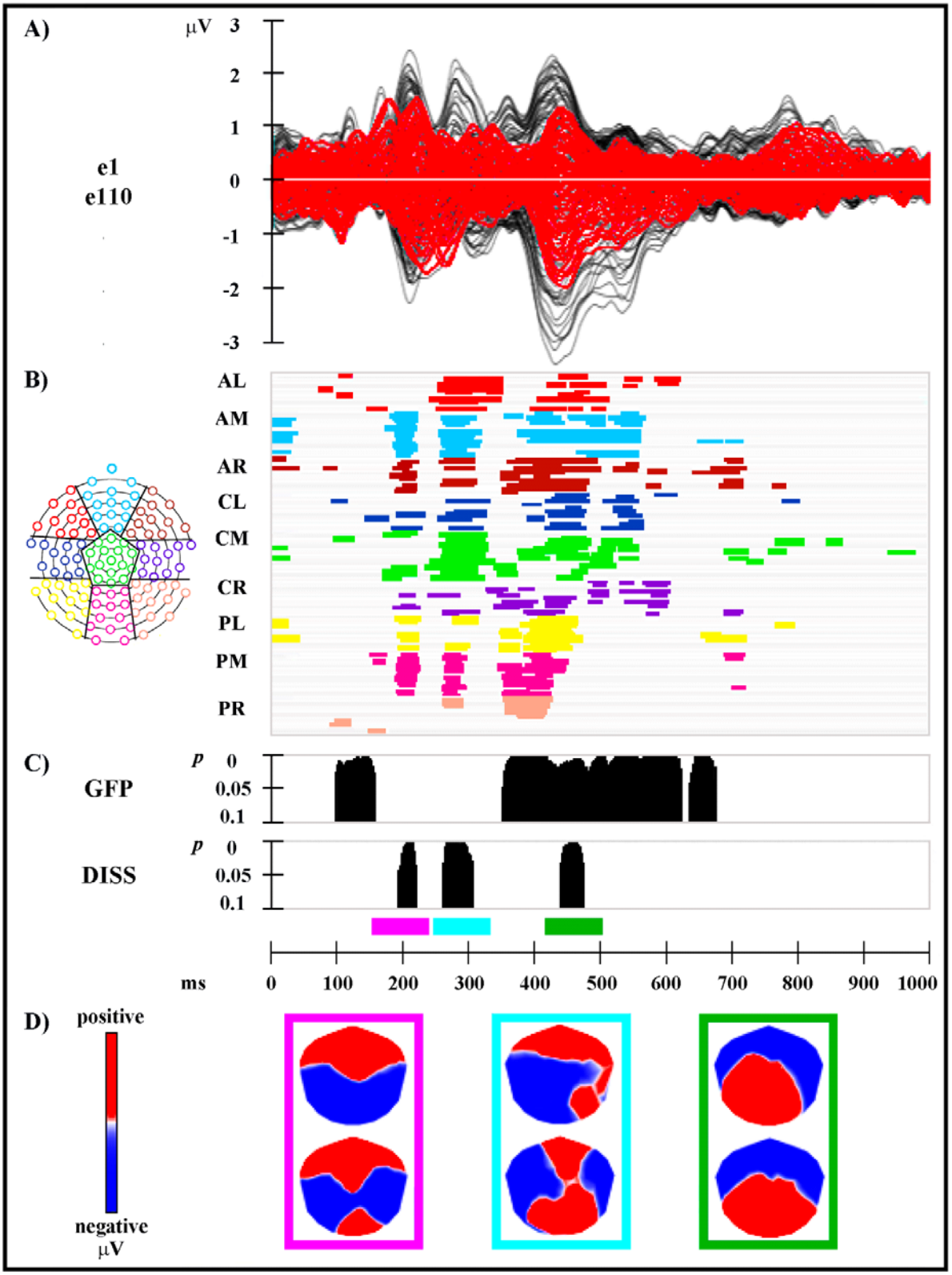
A)
μV
3
2
1
0
-1
-2
-3
e1
e110
B)
AL
AM
AR
CL
CM
CR
PL
PM
PR
C)
GFP
DISS
p
0
0.05
0.1
ms
0
100
200
300
400
500
600
700
800
900
1000
D)
positive
negative
μV

Figure 7. Electrophysiological results over 1000 ms after cue onset (cue onset: 0 ms).

A. Group-averaged (n = 15) event related potential (ERP) waveforms of the two experimental sessions, superimposed across the 110 recording channels (e1-e110). Black: session A; red: session B.

B. Statistical analysis of global ERP amplitude. Periods of significant differences of ERP amplitude ($p < .05$; duration $\geq$ 20 ms) at each electrode and time point between sessions are displayed as coloured horizontal lines. Each horizontal line represents one scalp electrode. Different colours indicate different clusters of electrodes; the distribution of the clusters over the electrode montage is shown in the inset on the left side of the figure. AL: anterior left; AM: anterior midline; AR: anterior right. CL: central left; CM: central midline; CR: central right. PL: posterior left; PM: posterior midline; PR: posterior right.

C. Global scalp electric field analyses. Upper plot: statistical analysis of global electric field strength. Black areas indicate time intervals of significant differences ($p < .05$; duration $\geq$ 20 ms) of Global Field Power (GFP) between sessions. Lower plot: statistical analysis of global electric field topography (topographic analysis of variance, TANOVA). Black areas indicate time intervals of significant differences ($p < .05$; duration $\geq$ 20 ms) of global map dissimilarity (DISS) between sessions.

D. Mean topographic maps of the group-averaged ERP data of session A (upper map) and session B (lower map), corresponding to each time interval of significant topographic modulation between sessions resulting from TANOVA. Each panel is coloured as the corresponding TANOVA time interval. All topographic maps are plotted with nasion upward and left scalp leftward; each map is scaled separately with respect to its maximum and minimum values to optimise the contrast.

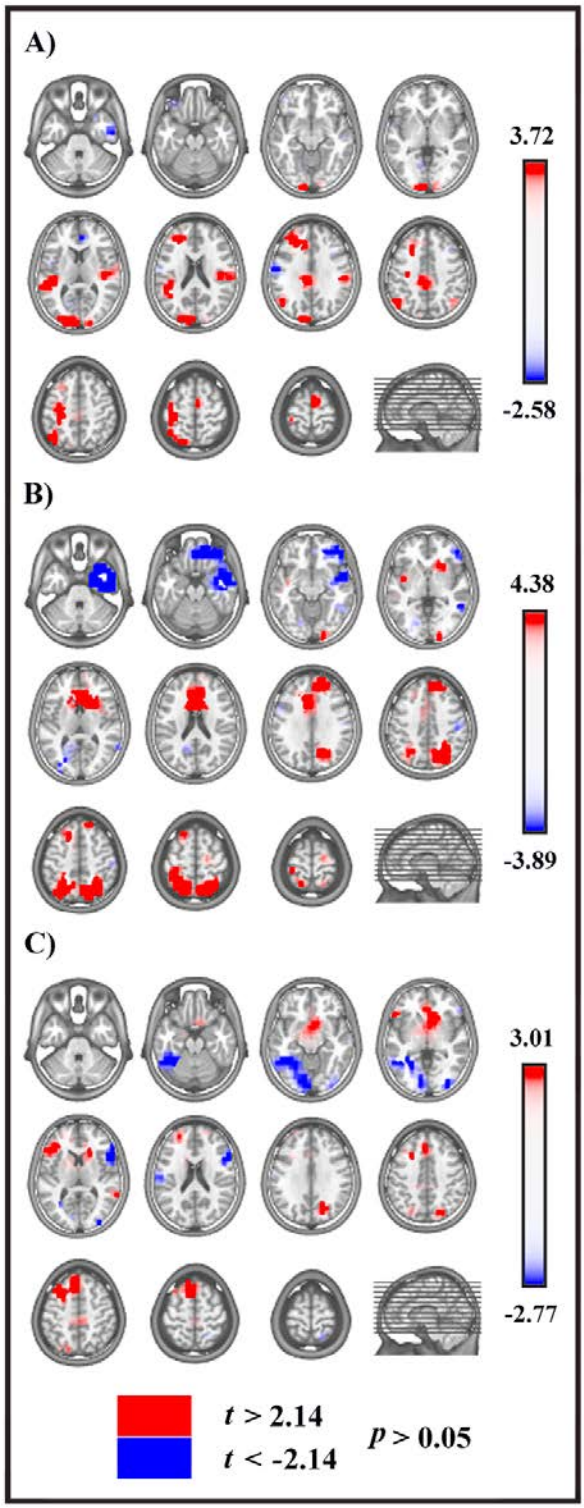
A)
3.72
-2.58
B)
4.38
-3.89
C)
3.01
-2.77
t > 2.14
t < -2.14
p > 0.05

Figure 8. Statistical comparisons of LAURA source estimations between session A and B over significant TANOVA time intervals. All significant voxels are coloured ($t_{(14)} > 2.14$ / < -2.14, $p < .05$): positive *t* values (red colour) indicate higher current source densities in session A than in session B; negative *t* values (blue colour) indicate higher current source densities in session B than in session A. LAURA solutions are rendered on MNI152 template brain (left hemisphere on the left side).

A. First significant TANOVA time interval (192-220 ms after cue onset).

B. Second significant TANOVA time interval (258-306 ms after cue onset).

C. Third significant TANOVA time interval (438-472 ms after cue onset).

Chapter 5

Conclusions and future directions

Taken together, the results of the analyses of preparatory and response phases of the present study demonstrate a substantial overlap of cerebral networks activated during proactive recruitment and subsequent reactive enactment of motor inhibition in both overt and covert actions. These findings suggest that the proposed strict cooperation between proactive and reactive inhibition required for a successful motor control of overt actions, could be also relevant in the covert motor context. At the same time, our data show a differential involvement of principal nodes of the proposed inhibitory network (namely, the pre-SMA and the rIFG), in accord with the intended modality of overt or covert motor response.

The analyses of the response phase in the Experimental Study Part 1 showed that covert actions as MI, automatically engage key nodes of the putative inhibitory circuit activated for the controlled inhibition of overt actions, triggered during the NoGo response by the inhibitory signal. On the one hand, these findings provide a possible mechanism allowing the covert nature of the imagined movement. On the other hand, our results further extend the proposed similarities of neural substrates of covert and overt actions [74] into the framework of motor inhibition. Nonetheless, our data underline that functional equivalence between overt and covert actions is only partial. Indeed, the shared cerebral substrates for the controlled inhibition of overt actions in NoGo condition and the automatic inhibition of covert actions in MI condition, showed different task-dependent functional interactions, in accord to the intended overt or covert modality of the motor response. The different temporal pattern of activation of the pre-SMA and rIFG in the overt and covert Go/NoGo tasks, suggested that an

inhibitory mechanism (likely underpinned by the rIFG) could be prewired into the selected covert motor performance modality, and triggered during the preparation for the covert Go/NoGo task.

In order to investigate how inhibition is included into the prepared covert mode of motor response, as a second step, the analyses of the preparatory phase in the Experimental Study Part 2 focused on the assessment of the specific cue-elicited cognitive strategies in our overt and covert Go/NoGo tasks.

During the preparation of the overt Go/NoGo task, the cue was encoded in a pragmatic mode: it primed the possible overt motor response programs in left motor cortex and dPMC. Of note, in the overt Go/NoGo task, the activation of the left dPMC emerged not only during the preparatory phase, but also in the following response phase during NoGo trials. Altogether, these findings are in line with previous evidence pointing to the role of the dPMC in both proactive [26] and reactive inhibition [24] of overt responses.

At the same time, during the overt Go/NoGo task, through preactivation of a pre-SMA-related "decisional" mechanism, the cue triggered a parallel preparation for the successful response selection and/or inhibition enacted during the subsequent response phase. Indeed, taking into account the whole overt Go/NoGo task, the pre-SMA engagement emerged during both the preparatory phase and the following NoGo response. Hence, our data support the involvement of the pre-SMA in both proactive and reactive inhibition of overt actions. These findings are consistent with previous evidence [e.g., 14-16, 18], and in particular with a human intracranial recording study, which found pre-SMA activation during the preparatory period and later on, just before movement inhibition [15].

Our analyses did not reveal the activation of the rIFG in the preparation of the overt Go/NoGo task; conversely, activation of the rIFG emerged during the subsequent NoGo response. These

results sustain a main role of the rIFG in reactive inhibitory control of overt actions, in line with previous evidence that did not find its proactive engagement [e.g., 14, 16-18].

Conversely, the cue-elicited activation of the rIFG emerged during the preparation of the covert Go/NoGo task. Indeed, the preparatory strategy for the covert Go/NoGo task was centered on the goal-oriented priming of an inhibitory mechanism related to the rIFG that, being tuned to the instructed covert type of the required motor response and instantiated during the subsequent MI enactment, allowed the imagined response to remain a potential motor act. Hence, during the preparatory phase of our cued overt and covert Go/NoGo tasks, the different adopted strategies are tuned to the "how" of the motor performance, reflecting the intended overt and covert modality of the possible incoming action.

In summary, the cue-triggered preparatory strategy for the overt Go/NoGo task prioritized the priming of the possible overt Go motor response (reflected in the left motor cortex and dPMC activation), and at the same time triggered a mechanism for the controlled response selection/inhibition of prepared response at the subsequent target onset (reflected in the pre-SMA activation). On the contrary, during the preparation for the covert Go/NoGo task, the cue elicited the priming of an inhibitory mechanism, pointing to a prioritized selection of how to perform the possible response at the incoming target (namely, with a covert movement). In addition, the reactive engagement of the left dPMC in the response phase during the MI performance could both reflect the actual rehearsal of the motor response and participate, together with other inhibitory nodes (the pre-SMA and the rIFG) to its automatic inhibition, maintaining the action covert.

Of note, our data showed an at least partial overlap in cerebral substrates for the controlled inhibition of overt actions in NoGo condition and the automatic inhibition of covert actions in MI condition. This is consistent with the growing literature [for reviews, see 149-151] that questions the traditional dichotomy between automatic (i.e., implicit, outside the phenomenal

awareness, conscious intention and volitional effort) and controlled (i.e., explicit, conscious, voluntary and cognitively effortful) cerebral processes [152, 153]. Our findings further suggest that automatic and unconscious motor control processes can form an intrinsic part of all voluntary, goal-oriented behaviours [125, 154].

In this regard, it is worth noting that MI is a particular type of covert action, in which the movement is voluntarily rehearsed and implicitly inhibited. However, even if inhibition runs to completion independently from intentionality and conscious control, it is included in the overall motor intention and consciously prepared in a goal-oriented manner, since subjects know that no overt movements have to be carried out during an imagined response. Our results encourage future research aimed at investigating whether and to which extent similar inhibitory mechanisms are implemented during other types of covert actions (for a taxonomical classification of covert actions, see [74]). Indeed, in different covert actions, such as during acion observation (AO), the activation of motor representations itself is automatically triggered by visual stimuli, not consciously retrieved: hence, these different type of covert actions could possibly entail different forms of automatic and implicit inhibition. Nonetheless, current evidence points toward the involvement in automatic inhibition during AO of brain areas similar to those emerged in the present data for the explicit inhibition of an overt response and the automatic inhibition of an imagined one (see "1.3 Motor inhibition and covert actions"). Future single-neuron recording studies should use paradigms including different covert action tasks (as MI and AO) and a voluntary movement withholding (NoGo task). This will greatly help to verify if common neural substrates are shared in different forms of inhibition of overt and covert actions, by comparing patterns of activity of the same neurons in various premotor regions in such different tasks.

References

1. Bari A, Robbins TW. Inhibition and impulsivity: behavioral and neural basis of response control. Prog Neurobiol. 2013; 108: 44-79.
2. Braver TS. The variable nature of cognitive control: a dual mechanisms framework. Trends Cogn Sci. 2012; 16: 106-113.
3. Aron AR. From reactive to proactive and selective control: developing a richer model for stopping inappropriate responses. Biol Psychiatry. 2011; 69: e55-68.
4. Alexander GE, Crutcher MD. Functional architecture of basal ganglia circuits: neural substrates of parallel processing. Trends Neurosci. 1990; 13: 266-271.
5. Nambu A, Tokuno H, Takada M. Functional significance of the cortico-subthalamo-pallidal 'hyperdirect' pathway. Neurosci Res. 2002; 43: 111-117.
6. Hampshire A, Chamberlain SR, Monti MM, Duncan J, Owen AM. The role of the right inferior frontal gyrus: inhibition and attentional control. Neuroimage. 2010; 50: 1313-1319.
7. Nachev P, Wydell H, O'neill K, Husain M, Kennard C. The role of the pre-supplementary motor area in the control of action. Neuroimage. 2007; 36: 155-163.
8. Mostofsky SH, Simmonds DJ. Response inhibition and response selection: two sides of the same coin. J Cogn Neurosci. 2008; 20: 751-761.
9. Isoda M, Hikosaka O. Switching from automatic to controlled action by monkey medial frontal cortex. Nat Neurosci. 2007; 10: 240-248.
10. Duann JR, Ide JS, Luo X, Li CS. Functional connectivity delineates distinct roles of the inferior frontal cortex and presupplementary motor area in stop signal inhibition. J Neurosci. 2009; 29: 10171-10179.

11. Neubert FX, Mars RB, Buch ER, Olivier E, Rushworth MF. Cortical and subcortical interactions during action reprogramming and their related white matter pathways. Proc Natl Acad Sci USA. 2010; 107: 13240-13245.

12. Mars RB, Klein MC, Neubert FX, Olivier E, Buch ER, Boorman ED, Rushworth MF Short-latency influence of medial frontal cortex on primary motor cortex during action selection under conflict. J Neurosci. 2009; 29: 6926-6931.

13. Buch ER, Mars RB, Boorman ED, Rushworth MF. A network centered on ventral premotor cortex exerts both facilitatory and inhibitory control over primary motor cortex during action reprogramming. J Neurosci. 2010; 30: 1395-1401.

14. Chikazoe J, Jimura K, Hirose S, Yamashita K, Miyashita Y, Konishi S. Preparation to inhibit a response complements response inhibition during performance of a stop-signal task. J Neurosci. 2009; 29: 15870-15877.

15. Swann NC, Cai W, Conner CR, Pieters TA, Claffey MP, George JS, Aron AR, Tandon N. Roles for the pre-supplementary motor area and the right inferior frontal gyrus in stopping action: electrophysiological responses and functional and structural connectivity. Neuroimage. 2012; 59: 2860-2870.

16. Majid DS, Cai W, Corey-Bloom J, Aron AR. Proactive selective response suppression is implemented via the basal ganglia. J Neurosci. 2013; 33: 13259-13269.

17. Zandbelt BB, Bloemendaal M, Neggers SFW, Kahn RS, Vink M. Expectations and violations: delineating the neural network of proactive inhibitory control. Hum Brain Mapp. 2013; 34: 2015-2024.

18. Van Belle J, Vinka M, Durston S, Zandbelt BB. Common and unique neural networks for proactive and reactive response inhibitions revealed by independent component analysis of functional MRI data. Neuroimage. 2014; 103: 65-74.

19. Verbruggen F, Aron AR, Stevens MA, Chambers CD. Theta burst stimulation dissociates attention and action updating in human inferior frontal cortex. Proc Natl Acad Sci USA. 2010; 107: 13966-13971.

20. Jahfari S, Stinear C, Claffey M, Verbruggen F, Aron A. Responding with restraint: what are the neurocognitive mechanisms? J Cogn Neurosci. 2010; 22:1479-1492.

21. Aron AR, Poldrack RA. Cortical and subcortical contributions to Stop signal response inhibition: role of the subthalamic nucleus. J Neurosci. 2006; 26:2424-2433.

22. Bogacz R, Wagenmakers EJ, Forstmann BU, Nieuwenhuis S. The neural basis of the speed- accuracy tradeoff. Trends Neurosci. 2010; 33:10-16.

23. Wise SP, Di Pellegrino G, Boussaoud D. The premotor cortex and nonstandard sensorimotor mapping. Can J Physiol Pharmacol. 1996; 74:469-482.

24. Mirabella G, Pani P, Ferraina S. Neural correlates of cognitive control of reaching movements in the dorsal premotor cortex of rhesus monkeys. J. Neurophysiol. 2011; 106: 1454-1466.

25. Mikuni N, Ohara S, Ikeda A, Hayashi N, Nishida N, Taki J, Enatsu R, Matsumoto R, Shibasaki H, Hashimoto N. Evidence for a wide distribution of negative motor areas in the perirolandic cortex. Clin Neurophysiol. 2006; 117:33-40.

26. Kalaska JF, Crammond DJ. Deciding not to go: neuronal correlates of response selection in a go/nogo task in primate premotor and parietal cortex. Cereb. Cortex. 1995; 5:410-428.

27. Criaud M., Boulinguez P. Have we been asking the right questions when assessing response inhibition in go/no-go tasks with fMRI? A meta-analysis and critical review. Neurosci Biobehav Rev. 2013; 37:11-23.

28. Riccio CA, Reynolds CR, Lowe P, Moore JJ. The continuous performance test: a window on the neural substrates for attention? Arch of Clin Neuropsychol. 2002; 17:235-272.

29. Rosvold H, Mirsky A, Sarason I, Bransome ED Jr, Beck LH. A continuous performance test of brain damage. J Consult Psychol. 1956; 20: 343-350.

30. Fallgatter AJ, Brandeis D, Strik WK. A robust assessment of the NoGo anteriorisation of P300 microstates in a cued Continuous Performance Test. Brain Topogr. 1997; 9:295-302.

31. Luck SJ. An introduction to the event-related potential technique. Cambridge, MA: MIT press; 2005.

32. Jodo E, Kayama Y. Relation of a negative ERP component to response inhibition in a Go/Nogo task. Electroencephalogr Clin Neurophysiol. 1992; 82: 477-482.

33. Fallgatter AJ, Strik WK. The NoGo-anteriorization as a neurophysiological standard-index for cognitive response control. Int J Psychophysiol. 1999; 32: 233-238.

34. Folstein JR, Van Petten C. Influence of cognitive control and mismatch on the N2 component of the ERP: a review. Psychophysiology. 2008; 45:152-170.

35. Nieuwenhuis S, Yeung N, van den Wildenberg W, Ridderinkhof KR. Electrophysiological correlates of anterior cingulate function in a go/no-go task: effects of response conflict and trial type frequency. Cogn Affect Behav Neurosci. 2003; 3:17-26.

36. Botvinick M, Cohen J, Carter C. Conflict monitoring and anterior cingulate cortex: an update. Trends Cogn Sci. 2004; 8:539-546.

37. Falkenstein M, Hoormann J, Hohnsbein J ERP components in Go/Nogo tasks and their relation to inhibition. Acta Psychologica 1999; 101: 267-291.

38. Kok A. Effects of degradation of visual stimulation on components of the event-related potential (ERP) in go/nogo reaction tasks. Biol Psychol. 1986; 23:21-38.

39. Polich J. Updating P300: an integrative theory of P3a and P3b. Clin Neurophysiol. 2007; 118:2128-2148.

40. Simson R, Vaughan HG, Ritter W. The scalp topography of potentials in auditory and visual go/nogo tasks. Electroenceph. Clin. Neurophysiol. 1977; 43: 864-875.

41. Verleger R. The true P3 is hard to see. Some comments on Kok's (1986) paper on degraded stimuli. Biol Psychol. 1988; 27: 45-50.

42. Pfefferbaum A, Ford JM, Weller BJ, Kopell BS. ERPs to response production and inhibition. Electroencephalogr Clin Neurophysiol. 1985; 60:423-434.

43. Kropotov JD, Ponomareva VA. Decomposing N2 NOGO wave of event-related potentials into independent components. Neuroreport. 2009; 20: 1592-1596.

44. Kropotov JD, Ponomarev VA, Hollup S, Mueller A. Dissociating action inhibition, conflict monitoring and sensory mismatch into independent components of event related potentials in GO/NOGO task. Neuroimage. 2011; 57: 565-575.

45. Huster RJ, Enriquez-Geppert S, Lavallee CF, Falkenstein M, Herrmann CS. Electroencephalography of response inhibition tasks: functional networks and cognitive contributions. Int J Psychophysiol. 2013; 87: 217-233.

46. Kiefer M, Marzinzik F, Weisbrod M, Scherg M, Spitzer M. The time course of brain activations during response inhibition: evidence from event-related potentials in a go/no go task. Neuroreport. 1998; 9: 765- 770.

47. Lavric A, Pizzagalli DA, Forstmeier S. When 'go' and 'nogo' are equally frequent: ERP components and cortical tomography. Eur J Neurosci. 2004; 20: 2483-2488.

48. Strik WK, Fallgatter AJ, Brandeis D, Pascual-Marqui RD. Three-dimensional tomography of event-related potentials during response inhibition: evidence for phasic frontal lobe activation. Electroenceph Clin Neurophysiol. 1998; 108: 406-413.

49. Bokura H, Yamaguchi S, Kobayashi S. Electrophysiological correlates for response inhibition in a Go/NoGo task. Clin Neurophysiol. 2001; 112: 2224-2232.

50. Michel CM, Thut G, Morand S, Khateb A, Pegna AJ, Grave de Peralta R, Gonzales S, Seeck M, Landis T. Electric source imaging of human brain functions. Brain Res Rev. 2001; 3: 108-118.

51. Dias EC, Foxe JJ, Javitt DC. Changing plans: a high density electrical mapping study of cortical control. Cereb Cortex. 2003; 13: 701-715.

52. Bekker EM, Kenemans JL, Verbaten MN. Electrophysiological correlates of attention, inhibition, sensitivity and bias in a continuous performance task. Clin Neurophysiol. 2004; 115: 2001-2013.

53. Brunia CH, van Boxtel GJ. Wait and see. Int J Psychophysiol. 2001; 43: 59-75.

54. Van Boxtel GJM, Böcker KBE. Cortical measures of anticipation. J. Psychophysiol. 2004; 18: 61-76.

55. Walter WG, Cooper R, Aldridge VJ, McCallum WC, Winter AL. Contingent negative variation: an electric sign of sensori-motor association and expectancy in the human brain. Nature. 1964; 203: 380-384.

56. Loveless NE, Sanford AJ. Effects of age on the contingent negative variation and preparatory set in a reaction time task. J Gerontol. 1974; 29: 52-63.

57. Loveless NE, Sanford AJ. The impact of warning signal intensity on reaction time and components of the contingent negative variation. Biol Psychol. 1975; 2: 217-226.

58. Gaillard AW. Effects of warning-signal modality on the contingent negative variation (CNV). Biol Psychol 1976; 4:139-154.

59. Rohrbaugh JW, Gaillard AWK. Sensory and motor aspects of the contingent negative variation. In: Gaillard AWK, Ritter W, editors. Tutorials in ERP research: Endogenous components. Amsterdam: North-Holland; 1983. pp. 269-310.

60. Kornhuber HH, Deecke L. Hirnpotentialänderungen bei Willkürbewegungen und passiven Bewegungen des Menschen: Bereitschaftspotential und reafferente Potentiale [Changes in the brain potential in voluntary movements and passive movements in man: readiness potential and reafferent potentials]. Pflugers Arch Gesamte Physiol Menschen Tiere. 1965; 284: 1-17.

61. Shibasaki H, Hallett M. What is the Bereitschaftspotential? Clin Neurophysiol. 2006; 117: 2341-2356.

62. Colebatch JG. Bereitschaftspotential and movement-related potentials: origin, significance, and application in disorders of human movement. Mov Disord. 2007; 22: 601-610.

63. Cunnington R, Iansek R, Bradshaw JL, Phillips JG. Movement-related potentials associated with movement preparation and motor imagery. Exp Brain Res. 1996; 111: 429-436.

64. Ikeda A, Shibasaki H, Kaji R, Terada K, Nagamine T, Honda M, Kimura J. Dissociation between contingent negative variation (CNV) and Bereitschaftspotential (BP) in patients with parkinsonism. Electroenceph Clin Neurophysiol. 1997; 102: 142-151.

65. Cui RQ, Egkher A, Huter D, Lang W, Lindinger G, Deecke L. High resolution spatiotemporal analysis of the contingent negative variation in simple or complex motor tasks and non-motor task. Clin. Neurophysiol. 2000; 111: 1847-1859.

66. Gómez CM, Marco J, Grau C. Preparatory visuo-motor cortical network of the contingent negative variation estimated by current density. Neuroimage. 2003; 20: 216-224.

67. Gómez CM, Flores A, Ledesma A. Fronto-parietal networks activation during the contingent negative variation period. Brain Res Bull. 2007; 73: 40-47.

68. Potts GF. An ERP index of task relevance evaluation of visual stimuli. Brain Cogn. 2004; 56: 5-13.

69. Banaschewski T, Brandeis D, Heinrich H, Albrecht B, Brunner E, Rothenberger A. Association of ADHD and conduct disorder--brain electrical evidence for the existence of a distinct subtype. J Child Psychol Psychiatry. 2003; 44: 356-376.

70. Boulinguez P, Ballanger B, Granjon L, Benraiss A. The paradoxical effect of warning on reaction time: demonstrating proactive response inhibition with event-related potentials. Clin Neurophysiol. 2009; 120: 730-737.

71. Kok A. The effect of warning stimulus novelty on the P300 and components of the contingent negative variation. Biol. Psychol. 1978; 6:219-233.

72. Brandeis D, Banaschewski T, Baving L, Georgiewa P, Blanz B, Warnke A, Steinhausen HC, Rothenberger A, Scheuerpflug P. Multicenter P300 brain mapping of impaired attention to cues in hyperkinetic children. J Am Acad Child Adolesc Psychiatry. 2002; 41: 990-998.

73. Jonkman LM. The development of preparation, conflict monitoring and inhibition from early childhood to young adulthood: a Go/Nogo ERP study. Brain Res. 2006; 1097: 181-193.

74. Jeannerod M. Neural simulation of action: a unifying mechanism for motor cognition. Neuroimage. 2001; 14: 103-109.

75. Gallese V, Fadiga L, Fogassi L, Rizzolatti G. Action recognition in the premotor cortex. Brain. 1996; 119: 593-609.

76. Fogassi L, Ferrari PF, Gesierich B, Rozzi S, Chersi F, Rizzolatti G. Parietal lobe: from action organization to intention understanding. Science. 2005; 29: 662-667.

77. Rizzolatti G, Craighero L. The mirror-neuron system. Annu Rev Neurosci. 2004; 27: 169-192.

78. Rizzolatti G, Sinigaglia C. The functional role of the parieto-frontal mirror circuit: interpretations and misinterpretations. Nat Rev Neurosci. 2010; 11: 264-274.

79. Jeannerod M, Decety J. Mental motor imagery: a window into the representational stages of action. Curr Opin Neurobiol. 1995; 5: 727-732.

80. Lotze M, Halsband U. Motor imagery. J Physiol Paris. 2006; 99: 386-395.

81. Guillot A, Collet C. Duration of mentally simulated movement: a review. J Mot Behav. 2005; 37: 10-20.

82. Munzert J, Lorey B, Zentgraf K. Cognitive motor processes: the role of motor imagery in the study of motor representations. Brain Res Rev. 2009; 60: 306-326.

83. Decety J, Jeannerod M, Germain M, Pastene J. Vegetative response during imagined movement is proportional to mental effort. Behav Brain Res. 1991; 42: 1-5.

84. Oishi K, Kasai T, Maeshima T. Autonomic response specificity during motor imagery. J Physiol Anthropol Appl Hum Sci. 2000; 19: 255-261.

85. Grezes J, Decety J. Functional anatomy of execution, mental simulation, observation, and verb generation of actions: a meta-analysis. Hum Brain Mapp. 2001; 12: 1-19.

86. Hanakawa T, Dimyan MA, Hallett M. Motor planning, imagery, and execution in the distributed motor network: a time-courses study with functional MRI. Cereb Cortex. 2008; 18: 2775-2788.

87. Macuga KL, Frey SH. Neural representations involved in observed, imagined, and imitated actions are dissociable and hierarchically organized. Neuroimage. 2012; 59: 2798-2807.

88. Jankelowitz SK, Colebatch JG. Movement-related potentials associated with selfpaced, cued and imagined arm movements. Exp Brain Res. 2002; 147: 98-107.

89. Caldara R, Deiber MP, Andrey C, Michel CM, Thut G, Hauert CA. Actual and mental motor preparation and execution: a spatiotemporal ERP study. Exp Brain Res. 2004; 159: 389-399.

90. Galdo-Alvarez S, Carrillo-de-la-Peña MT. ERP evidence of MI activation without motor response execution. Neuroreport. 2004; 15:2067-2070.

91. Carrillo-de-la-Pena MT, Galdo-Alvarez S, Lastra-Barreira C. Equivalent is not equal: primary motor cortex (MI) activation during motor imagery and execution of sequential movements. Brain Res. 2008; 1126: 134-143.

92. Kranczioch C, Mathews S, Dean PJ, Sterr A. On the equivalence of executed and imagined movements: evidence from lateralized motor and nonmotor potentials. Hum Brain Mapp. 2009; 30: 3275-3286.

93. Kranczioch C, Mathews S, Dean P, Sterr A. Task complexity differentially affects executed and imagined movement preparation: evidence from movement-related potentials. PLoSOne. 2010; 5:e9284.

94. De Jong R, Coles MG, Logan GD, Gratton G. In search of the point of no return: the control of response processes. J Exp Psychol Hum Percept Perform. 1990; 16: 164-182.

95. Dum RP, Strick PL. The origin of corticospinal projections from the premotor areas in the frontal lobe. J Neurosci. 1991; 11: 667-689.

96. Solodkin A, Hlustik P, Chen EE, Small SL. Fine modulation in network activation during motor execution and motor imagery. Cereb Cortex. 2004; 14: 1246-1255-

97. Kasess CH, Windischberger C, Cunnington R, Lanzenberger R, Pezawas L, Moser E. The suppressive influence of SMA on M1 in motor imagery revealed by fMRI and dynamic causal modeling. Neuroimage. 2008; 40: 828-837.

98. Raos V, Evangeliou MN, Savaki HE. Mental simulation of action in the service of action perception. J Neurosci. 2007; 27: 12675-12683.

99. Stamos AV, Savaki HE, Raos V. The spinal substrate of the suppression of action during action observation. J Neurosci. 2010; 30: 11605-11611.

100. Kraskov A, Dancause N, Quallo MM, Shepherd S, Lemon RN. Corticospinal neurons in macaque ventral premotor cortex with mirror properties: a potential mechanism for action suppression? Neuron. 2009; 64: 922-930.

101. Mukamel R, Ekstrom AD, Kaplan J, Iacoboni M, Fried I. Single-neuron responses in humans during execution and observation of actions. Curr Biol. 2010; 20: 750-756.

102. Vigneswaran G, Philipp R, Lemon RN, Kraskov A. M1 corticospinal mirror neurons and their role in movement suppression during Action Observation. Curr Biol. 2013; 23: 236-243.

103. Hohlefeld FU, Nikulin VV, Curio G. Visual stimuli evoke rapid activation (120 ms) of sensorimotor cortex for overt but not for covert movements. Brain Res. 2011; 1368: 185-195.

104. Picton TW, Bentin S, Berg P, Donchin E, Hillyard SA, Johnson R Jr, Miller GA, Ritter W, Ruchkin DS, Rugg MD, Taylor MJ. Guidelines for using human event-related potentials to study cognition: recording standards and publication criteria. Psychophysiology. 2000; 37: 127-152.

105. Murray MM, Brunet D, Michel CM. Topographic ERP analyses: a step-by-step tutorial review. Brain Topogr. 2008; 20: 249-264.

106. Lehmann D. Principles of spatial analysis. In: Gevins AS, Remond A, editors. Handbook of electroencephalography and clinical neurophysiology, vol. 1: methods of analysis of brain electrical and magnetic signals. Amsterdam: Elsevier; 1987. pp. 309-354.

107. Michel CM, Koenig T, Thomas CM, Brandeis D, Gianotti LRR, Wackermann J, editors. Electrical Neuroimaging. Cambridge (UK): Cambridge University Press; 2009.

108. Oldfield R. The assessment and analysis of handedness: the Edinburgh inventory. Neuropsychologia. 1971; 9: 97-113.

109. Fallgatter AJ, Bartsch AJ, Strik WK, Mueller TJ, Eisenack SS, Neuhauser B, Aranda D, Herrmann MJ. Test-retest reliability of electrophysiological parameters related to cognitive motor control. Clin Neurophysiol. 2001; 112: 198-204.

110. Kirmizi-Alsan E, Bayraktaroglu Z, Gurvit H, Keskin YH, Emre M, Demiralp T. Comparative analysis of event-related potentials during Go/NoGo and CPT: decomposition of electrophysiological markers of response inhibition and sustained attention. Brain Res. 2006; 1104: 114-128.

111. Brunet D, Murray MM, Michel CM. Spatiotemporal analysis of multichannel EEG: CARTOOL. Comput Intell Neurosci. 2011; 2011: 813870.

112. Perrin F, Pernier J, Bertrand O, Giard MH, Echallier JF. Mapping of scalp potentials by surface spline interpolation. Electroenceph Clin Neurophysiol. 1987; 66: 75-78.

113. Isaac AR, Marks DF, Russell DG. An instrument for assessing imagery of movement: The Vividness of Movement Imagery Questionnaire (VMIQ). Journal of Mental Imagery. 1986; 10: 23-30.

114. Michel CM, Murray MM, Lantz G, Gonzalez S, Spinelli L, Grave de Peralta R. EEG source imaging. Clin Neurophysiol. 2004; 115: 2195-2222.

115. Koenig T, Prichep L, Lehmann D, Sosa PV, Braeker E, Kleinlogel H, Isenhart R, John ER. Millisecond by millisecond, year by year: normative EEG microstates and developmental stages. Neuroimage 2002; 16: 41-48.

116. Krzanowski W, Lai YT. A criterion for determining the number of groups in a data set using sum of squares clustering. Biometrics. 1985; 44: 23-34.

117. Grave De Peralta Menendez R, Andino SG, Lantz G, Michel CM, Landis T. Noninvasive localization of electromagnetic epileptic activity. I. Method descriptions and simulations. Brain Topogr. 2001; 14: 131- 137.

118. Spinelli L, Andino SG, Lantz G, Seeck M, Michel CM. Electromagnetic inverse solutions in anatomically constrained spherical head models. Brain Topogr. 2000; 13: 115-125.

119. Talairach J, Tournoux P. Co-planar stereotaxic atlas of the human brain. New York (NY): Thieme Medical Publisher; 1988.

120. Cisek P, Kalaska JF. Neural mechanisms for interacting with a world full of action choices. Annu Rev Neurosci. 2010; 33: 269-298.

121. Miller EK. The prefrontal cortex and cognitive control. Nat Rev Neurosci. 2000; 1: 59-65.

122. Simmonds DJ, Pekar JJ, Mostofsky SH. Meta-analysis of Go/No-go tasks demonstrating that fMRI activation associated with response inhibition is task-dependent. Neuropsychologia. 2008; 46: 224-232.

123. Corbetta M, Shulman GL. Control of goal-directed and stimulus-driven attention in the brain. Nat Rev Neurosci. 2002; 3: 201-215.

124. Anderson EJ, Husain M, Sumner P. Human intraparietal sulcus (IPS) and competition between exogenous and endogenous saccade plans. Neuroimage. 2008; 40: 838-851.

125. Sumner P, Husain M. At the edge of consciousness: automatic motor activation and voluntary control. Neuroscientist. 2008; 14: 474-486.

126. Hoshi E, Tanji J. Distinctions between dorsal and ventral premotor areas: anatomical connectivity and functional properties. Curr Opin Neurobiol. 2007; 17: 234-242.

127. Endo H, Kizuka T, Masuda T, Takeda T. Automatic activation in the human primary motor cortex synchronized with movement preparation. Cogn Brain Res. 1999; 3: 229-239.

128. Duque J, Lew D, Mazzocchio R, Olivier E, Ivry RB. Evidence for two concurrent inhibitory mechanisms during response preparation. J Neurosci. 2010; 30: 3793-3802.

129. Watanabe J, Sugiura M, Sato K, Sato Y, Maeda Y, Matsue Y, Fukuda H, Kawashima R. The human prefrontal and parietal association cortices are involved in NO-GO performances: an event-related fMRI study. Neuroimage. 2002; 17: 1207-1216.

130. Filevich E, Kühn S, Haggard P. Negative motor phenomena in cortical stimulation: implications for inhibitory control of human action. Cortex. 2012; 48: 1251-1261.

131. Rizzolatti G, Luppino G, Matelli M. The classic supplementary motor area is formed by two independent areas. Adv Neurol. 1996; 70: 45-56.

132. Duque J, Olivier E, Rushworth M. Top-down inhibitory control exerted by the medial frontal cortex during action selection under conflict. J Cogn Neurosci. 2013; 25: 1634-1648.

133. Aron AR, Robbins TW, Poldrack RA. Inhibition and the right inferior frontal cortex: one decade on. Trends Cogn Sci. 2014; 18: 177-185.

134. Sharp DJ, Bonnelle V, De Boissezon X, Beckmann CF, James SG, Patel MC, Mehta MA. Distinct frontal systems for response inhibition, attentional capture, and error processing. Proc Natl Acad Sci USA. 2010; 107: 6106-6111.

135. Bargh JA. Conditional automaticity: varieties of automatic influences in social perception and cognition. In: Uleman JS, Bargh JA, editors. Unintended Thought. New York (NY): Guilford Press; 1989. pp. 3-51.

136. Anderson BA, Folk CL. Conditional automaticity in response selection: contingent involuntary response inhibition with varied stimulus-response mapping. Psychol Sci. 2014; 25: 547-554.

137. Lenartowicz A, Verbruggen F, Logan GD, Poldrack RA. Inhibition-related activation in the right inferior frontal gyrus in the absence of inhibitory cues. J Cogn Neurosci. 2011; 23: 3388-3399.

138. Van Gaal S, Ridderinkhof KR, Scholte HS, Lamme VA. Unconscious activation of the prefrontal no-go network. J Neurosci. 2010; 30: 4143-4150.

139. Chiu YC, Aron AR. Unconsciously triggered response inhibition requires an executive setting. J Exp Psychol. 2014; 143: 56-61.

140. Jaffard M, Longcamp M, Velay JL, Anton JL, Roth M, Nazarian B, Boulinguez P. Proactive inhibitory control of movement assessed by event-related fMRI. Neuroimage. 2008; 42: 1196-1206.

141. Koenig T, Melie-Garcia L. “Statistical analysis of multichannel scalp field data” in: Electrical Neuroimaging. Michel CM, Koenig T, Brandeis D, Gianotti LRR, Wackermann J, editors. Cambridge (UK): Cambridge University Press; 2009. pp.170-172,

142. Manly BF. Randomization and Monte Carlo methods in biology. London (UK): Chapman & Hall; 1991.

143. Guthrie D, Buchwald JS. Significance testing of difference potentials. Psychophysiology. 1991; 28:240-244.

144. Jaffard M, Benraiss A, Longcamp M, Velay JL, Boulinguez P. Cueing method biases in visual detection studies. Brain Res. 2007; 1179:106-118.

145. Boulinguez P, Jaffard M, Granjon L, Benraiss A. Warning signal induce automatic EMG activation and proactive volitional inhibition: evidence from the analysis of error distribution in simple RT. J Neurophysiol. 2008; 99:1572-1578.

146. Carter CS, Botvinick MM, Cohen JD. The contribution of the anterior cingulate cortex to executive processes in cognition. Rev Neurosci. 1999; 10:49-57

147. Chen X, Scangos KW, Stuphorn V. Supplementary motor area exerts proactive and reactive control of arm movements. J Neurosci. 2010; 30:14657-14675.

148. Stuphorn V, Emeric EE. Proactive and reactive control by the medial frontal cortex. Front Neuroeng. 2012; 5:9.

149. Hommel B. Consciousness and control: not identical twins. J Conscious Stud. 2007; 14: 155-167.

150. Verbruggen F, Best M, Bowditch WA, Stevens T, McLaren IP. The inhibitory control reflex. Neuropsychologia. 2014; 65: 263-278.

151. Verbruggen F, McLaren IP, Chambers CD. Banishing the control homunculi in studies of action control and behavior change. Perspect Psychol Sci. 2014; 9: 497-524.

152. Schneider W, Shiffrin RM. Controlled and automatic human information processing: I. Detection, search, and attention. Psychol Rev. 1977; 84: 1-66.

153. Shiffrin RM, Schneider W. Controlled and automatic human information processing: II. Perceptual learning, automatic attending and a general theory. Psychol Rev. 1977; 84: 127-190.

154. McBride J, Boy F, Husain M, Sumner P. Automatic motor activation in the executive control of action. Front Hum Neurosci. 2012; 6: 82.